

This discussion paper is/has been under review for the journal Atmospheric Measurement Techniques (AMT). Please refer to the corresponding final paper in AMT if available.

# Profiles of CH<sub>4</sub>, HDO, H<sub>2</sub>O, and N<sub>2</sub>O with improved lower tropospheric vertical resolution from Aura TES radiances

J. Worden<sup>1</sup>, S. Kulawik<sup>1</sup>, C. Frankenberg<sup>1</sup>, V. Payne<sup>2</sup>, K. Bowman<sup>1</sup>,  
K. Cady-Peirara<sup>2</sup>, K. Wecht<sup>3</sup>, J.-E. Lee<sup>1</sup>, and D. Noone<sup>4</sup>

<sup>1</sup>Jet Propulsion Laboratory/California Institute of Technology, Pasadena, CA, USA

<sup>2</sup>Atmospheric and Environmental Research, Lexington, MA, USA

<sup>3</sup>Earth and Planetary Sciences, Harvard University, MA, USA

<sup>4</sup>Department of Atmospheric and Oceanic Sciences, and Cooperative Institute for Research in Environmental Sciences, University of Colorado, Boulder, CO, USA

Received: 21 August 2011 – Accepted: 18 October 2011 – Published: 3 November 2011

Correspondence to: J. Worden (john.worden@jpl.nasa.gov)

Published by Copernicus Publications on behalf of the European Geosciences Union.

Title Page

Abstract

Introduction

Conclusions

References

Tables

Figures

◀

▶

◀

▶

Back

Close

Full Screen / Esc

Printer-friendly Version

Interactive Discussion



## Abstract

Thermal infrared (IR) radiances measured near 8 microns contain information about the vertical distribution of water vapor ( $\text{H}_2\text{O}$ ), one of its minor isotopologues (HDO) and methane ( $\text{CH}_4$ ), key gases that can be used to investigate the water and carbon cycles. Here, we show improvements in vertical resolution and reduction in uncertainties for estimates of these trace gases made from the Aura Tropospheric Emission Spectrometer (TES). The improvements are achieved by utilizing more of the inherent information available in the TES measurements. In previous versions of the TES profile retrieval algorithm, a “spectral-window” approach was used that attempted to minimize uncertainty from interfering species. However, this approach can also reduce the vertical resolution of the retrieved species. Here we document the vertical sensitivity and error characteristics of retrievals in which  $\text{H}_2\text{O}$ , HDO,  $\text{CH}_4$  and nitrous oxide ( $\text{N}_2\text{O}$ ) are jointly estimated (together with temperature, surface emissivity, and cloud properties) using the spectral region between  $1100\text{ cm}^{-1}$  and  $1330\text{ cm}^{-1}$ . The TES retrieval constraints are also modified to maximize the use of this information. The  $\text{H}_2\text{O}$  estimates show greater vertical resolution in the lower troposphere and boundary layer, while the new HDO/ $\text{H}_2\text{O}$  estimates can now profile the HDO/ $\text{H}_2\text{O}$  ratio between 925 hPa and 450 hPa in the tropics and during summertime at high latitudes. The new retrievals are now sensitive to methane in the free troposphere between 800 and 150 mb with peak sensitivity near 650 hPa. However, there is a bias in the upper troposphere of approximately 10 % that is likely related to temperature uncertainties and/or to errors in the methane spectroscopy. We discuss approaches for correcting this bias either through averaging or through correcting the estimated methane using co-estimated  $\text{N}_2\text{O}$  profiles. While these new  $\text{CH}_4$ , HDO/ $\text{H}_2\text{O}$ , and  $\text{H}_2\text{O}$  estimates are consistent with previous TES retrievals in the regions of overlap, future comparisons with independent profile measurement will be required to validate these new retrievals.

## Profiles of $\text{CH}_4$ , HDO, $\text{H}_2\text{O}$ , and $\text{N}_2\text{O}$

J. Worden et al.

Title Page

Abstract

Introduction

Conclusions

References

Tables

Figures

◀

▶

◀

▶

Back

Close

Full Screen / Esc

Printer-friendly Version

Interactive Discussion



## 1 Introduction

Investigating the processes controlling the water and carbon cycles and their linkages require multiple tracers that are sensitive to the vertically distributed sources, sinks, and processes controlling the water and carbon cycles. For example, Fig. 1a shows a schematic (Brown, 2011) of the vertical distribution of moisture sources, sinks, and exchange processes in the troposphere. Measurements of water vapor profiles (e.g., Dessler et al., 2007, and references therein), upper tropospheric water (e.g., Reed et al., 2008) and the vertical distribution of clouds (e.g., Stephens and Vane, 2007; Su et al., 2008) have been used to examine the exchange and transport processes controlling tropospheric humidity. Measurements of the isotopic ratio of water can provide an additional constraint for quantifying the distribution of the sources and exchange processes through the sensitivity of this composition to that of the moisture source, to changes in phase, and to transport and mixing processes (e.g., Kuang et al., 2003; Worden et al., 2006, 2007; Risi et al., 2008; Nassar et al., 2007; Payne et al., 2007; Brown et al., 2008; Noone et al., 2008; Frankenberg et al., 2009; Herbin et al., 2009; Steinwagner et al., 2010). Satellite measurements such as those from TES, the Atmospheric Chemistry Experiment (ACE), the Infrared Atmospheric Sounding Interferometer (IASI), and the SCanning Imaging Absorption SpectroMeter for Atmospheric CHartographY (SCIAMACHY) have been used for this purpose. Similarly, any of the dynamical processes controlling the water cycle such as surface exchange, mixing, advection, and convection also affect the carbon cycle. Figure 1b shows a schematic of the sources, sinks, and dynamics affecting atmospheric CO<sub>2</sub> and CH<sub>4</sub> methane (adopted from Sarrat et al., 2010). As with water, mixing processes in the free troposphere (e.g., Jiang et al., 2008; Li et al., 2010; Lee et al., 2007; Risi et al., 2008) and boundary layer (e.g., Stephens et al., 2007a; Picket-Heaps et al., 2011; Querino et al., 2011) affect the tropospheric distribution of CO<sub>2</sub> (Nassar et al., 2011) and CH<sub>4</sub> and must be accounted for when estimating fluxes and emissions.

AMTD

4, 6679–6721, 2011

### Profiles of CH<sub>4</sub>, HDO, H<sub>2</sub>O, and N<sub>2</sub>O

J. Worden et al.

Title Page

Abstract

Introduction

Conclusions

References

Tables

Figures

◀

▶

◀

▶

Back

Close

Full Screen / Esc

Printer-friendly Version

Interactive Discussion



---

**Profiles of CH<sub>4</sub>, HDO,  
H<sub>2</sub>O, and N<sub>2</sub>O**J. Worden et al.

---

[Title Page](#)[Abstract](#)[Introduction](#)[Conclusions](#)[References](#)[Tables](#)[Figures](#)[◀](#)[▶](#)[◀](#)[▶](#)[Back](#)[Close](#)[Full Screen / Esc](#)[Printer-friendly Version](#)[Interactive Discussion](#)

Consequently, in order to investigate the processes, sources, and sinks affecting the global carbon and water cycles it is useful to have vertically resolved trace gas profiles. It is with this motivation that we seek to improve the vertical resolution of the TES H<sub>2</sub>O, HDO, and CH<sub>4</sub> products, especially in the lowermost troposphere and boundary layer where many of the exchange processes between the surface, boundary layer, and free troposphere have significant impact on the tropospheric distribution of these gases.

In this paper we show that a simultaneous retrieval of H<sub>2</sub>O, HDO, CH<sub>4</sub> and N<sub>2</sub>O using spectral radiances from the TES instrument (Beer et al., 2001) between 1150 and 1340 cm<sup>-1</sup> will result in improved vertical resolution and uncertainties for TES geophysical retrievals over the previous TES results. We first present an overview of the previous (use of spectral micro-windows to minimize interference errors) and new (joint estimate) TES retrieval approaches. We then present an overview of the error characteristics and vertical resolution for H<sub>2</sub>O, HDO/H<sub>2</sub>O and CH<sub>4</sub> profiles. We also show how referencing the estimated methane profile to the jointly retrieved N<sub>2</sub>O results can theoretically reduce systematic errors, most notably from temperature, in the methane profile estimate; however, improved a priori distributions of N<sub>2</sub>O are required before we fully exploit this potential error reduction. Comparisons between the new and old estimates are shown in the altitude regions where the sensitivities overlap for HDO and H<sub>2</sub>O. Validation of the new retrievals where vertical sensitivity has been increased will be discussed in subsequent papers.

## 2 The TES instrument and trace gas retrieval overview

The TES instrument is an infrared, high spectral resolution, Fourier Transform spectrometer covering the spectral range between 650 to 3050 cm<sup>-1</sup> (15.4 to 3.3 μm) with an apodized spectral resolution of 0.1 cm<sup>-1</sup> for the nadir view (Beer et al., 2001). Spectral radiances measured by TES are used to infer atmospheric profiles using a non-linear optimal estimation algorithm that minimizes the difference between these radiances and those calculated with the equation of radiative transfer (Clough et al.,

2006), subject to the constraint that the parameters are consistent with a statistical a priori description of the atmosphere (Rodgers, 2000; Bowman et al., 2006). TES provides a global view of tropospheric trace gas profiles including ozone, water vapor and its isotopes, carbon monoxide and methane, along with atmospheric temperature, surface temperature, surface emissivity, effective cloud top pressure, and effective cloud optical depth (Worden et al., 2004; Kulawik et al., 2006b; Eldering et al., 2007).

### 3 Retrieval approach

#### 3.1 Spectral windows

A common approach when performing retrievals from high resolution Fourier transform spectrometers such as TES is to select spectral windows for each target atmospheric constituent that maximize information gained from a spectral measurement and minimize the systematic errors related to incorrect knowledge of temperature, emissivity, spectral errors, or radiative interference from un-retrieved species (e.g., Echle et al., 2000; Dudhia et al., 2002; Worden et al., 2004; Kuai et al., 2010). The details of the approach for the TES spectral window selection are described in Worden et al. (2004). The general procedure is to first compute an error budget for a set of spectral windows using the following equation:

$$\hat{x} = x_a + A_{xx}(x - x_a) + A_{xy}(y - y_a) \mathbf{M} \mathbf{G}_z \mathbf{m} + \sum_i \mathbf{M} \mathbf{G}_z \mathbf{K}_b^i (b^i - b_a^i) \quad (1)$$

where  $\hat{x}$  is the estimate of interest and the subscript “a” indicates that a priori knowledge is used for the corresponding vector. The  $\mathbf{A}_{xx}$  is the averaging kernel matrix describing the sensitivity of the estimate to the true state:  $\mathbf{A} = \frac{\partial \hat{x}}{\partial x}$ . The  $\mathbf{A}_{xy}$  is the sensitivity of  $x$  to other parameters ( $y$ ) that are jointly estimated with  $\hat{x}$ . The  $\mathbf{M}$  is a mapping matrix relating retrieval parameters  $z$  back to the full profile  $x$ ,  $x = \mathbf{M}z$  (many retrievals use a subset of parameters as a hard constraint to regularize the retrieval

Title Page

Abstract

Introduction

Conclusions

References

Tables

Figures

◀

▶

◀

▶

Back

Close

Full Screen / Esc

Printer-friendly Version

Interactive Discussion



## Profiles of CH<sub>4</sub>, HDO, H<sub>2</sub>O, and N<sub>2</sub>O

J. Worden et al.

Title Page

Abstract

Introduction

Conclusions

References

Tables

Figures

◀

▶

◀

▶

Back

Close

Full Screen / Esc

Printer-friendly Version

Interactive Discussion



as discussed in Worden et al., 2004, and Bowman et al., 2006). The vector  $m$  is the measurement noise as a function of wavelength. The  $b$  term represents un-retrieved parameters that affect the observed radiance with  $\mathbf{K}_b$  being the Jacobian or sensitivity of those terms to the radiance. The  $\mathbf{G}$  is the gain matrix, which is the partial derivative of the retrieval parameters to the radiance ( $\mathbf{F}$ ):

$$\mathbf{G}_z = \frac{\partial z}{\partial \mathbf{F}} = \left( \mathbf{K}_z^T \mathbf{S}_m^{-1} \mathbf{K}_z + \mathbf{\Lambda}_z \right)^{-1} \mathbf{K}_z^T \mathbf{S}_m^{-1}, \quad (2)$$

where  $\mathbf{S}_m$  is the covariance of the measurement noise for an ensemble of measurements and  $\mathbf{\Lambda}_z$  is a constraint matrix used to regularize the retrieval.

The last term in Eq. (1) is the sum over all terms that are not retrieved with the state vector  $x$  but which also affect the measured or modeled radiance. Since in general the noise vector and the errors in these parameters are not exactly known we instead estimate their second order statistics to calculate the errors in  $x$  from each term:

$$\mathbf{S}_{\text{tot}} = (\mathbf{A}_{xx} - \mathbf{I}) \mathbf{S}_a (\mathbf{A}_{xx} - \mathbf{I})^T + \mathbf{A}_{xy} \mathbf{S}_y \mathbf{A}_{xy}^T + \mathbf{S}_m + \sum_i \mathbf{S}_i^b \quad (3)$$

where these four terms correspond to the terms in Eq. (1):  $\mathbf{S}_{\text{tot}}$  is the total error, the next term dependent on  $\mathbf{S}_a$  is the “smoothing error” which describes how well the estimate can infer the natural variability of the atmosphere (Rodgers, 2000). The third term depending on  $\mathbf{S}_y$  is similar to the smoothing error and characterizes the impact of the natural variability of jointly estimated parameters on the parameters of interest (Worden et al., 2004). The  $\mathbf{S}_M$  is the measurement error related to noise, and the summation is over all un-retrieved parameters ( $b$ ) which could include spectroscopic uncertainties, temperature, or un-retrieved species.

In general, spectral window selection involves calculating whether a measurement adds information (using a definition of Shannon information content that is related to a decreases uncertainty) using the following equation:

$$\Delta \mathbf{H} = \frac{1}{2} \log_2 \left( \frac{|\mathbf{S}_{x1}|}{|\mathbf{S}_{x2}|} \right) = \frac{1}{2} (\log_2 |\mathbf{S}_{x1}| - \log_2 |\mathbf{S}_{x2}|) \quad (4)$$

where  $\mathbf{H}$  is the information content,  $\mathbf{S}_{x1}$  is the error covariance before adding a measurement and  $\mathbf{S}_{x2}$  is the error covariance after adding a measurement.

For the previous TES methane retrieval, HDO, H<sub>2</sub>O, and N<sub>2</sub>O were treated as radiatively interfering species, and similarly CH<sub>4</sub> was considered to interfere with the spectral features of H<sub>2</sub>O and HDO. For example, if a given spectral point measurement were highly sensitive to methane then it would add uncertainty (as shown in Eq. 1) to the HDO/H<sub>2</sub>O retrieval. The net information gain (Eq. 4) would likely be negative for the HDO/H<sub>2</sub>O estimate and that spectral point would not be used. To illustrate this problem, Fig. 2a and b shows TES measured radiances and calculated Jacobians for CH<sub>4</sub>, N<sub>2</sub>O, H<sub>2</sub>O, and HDO for a tropical ocean scene. The Jacobians have been normalized by the TES measurement noise and integrated over the whole atmospheric column. The spectral regions colored in red are the spectral regions used for TES v5 retrievals. The CH<sub>4</sub> windows were selected to the methane window reduce interferences from H<sub>2</sub>O and HDO. N<sub>2</sub>O lines are present throughout the CH<sub>4</sub> region and are practically impossible to window around. Similarly, the spectral windows for HDO and H<sub>2</sub>O were selected to reduce interference from CH<sub>4</sub>. Figure 2a and b also illustrates high sensitivity to CH<sub>4</sub> illustrates that, HDO, H<sub>2</sub>O, and N<sub>2</sub>O across a wide region. In order to make full use of the spectral information available without negatively adding information content it is necessary to jointly retrieve all constituents together (Worden et al., 2004). If all constituents are jointly retrieved then the last term in Eq. (3) becomes zero and all data points increase the information content. Our approach then is to use effectively the entire spectral range shown in Fig. 2 to jointly estimate HDO, H<sub>2</sub>O, N<sub>2</sub>O, and methane. However, we currently avoid the a 10 cm<sup>-1</sup> wide spectral region centered around 1280 cm<sup>-1</sup> which contains a strong CFC line that is not currently in our atmospheric radiation transfer (forward) model. Other interfering species such as CO<sub>2</sub>, O<sub>3</sub>, and HNO<sub>3</sub> are included in our forward model and the errors from these species are included in our error calculation.

**Profiles of CH<sub>4</sub>, HDO,  
H<sub>2</sub>O, and N<sub>2</sub>O**

J. Worden et al.

Title Page

Abstract

Introduction

Conclusions

References

Tables

Figures

I◀

▶I

◀

▶

Back

Close

Full Screen / Esc

Printer-friendly Version

Interactive Discussion



## 3.2 State vector

The new state vector for this joint estimate is:

$$\mathbf{x} = \begin{bmatrix} X_{\text{H}_2\text{O}} \\ X_{\text{HDO}} \\ X_{\text{CH}_4} \\ X_{\text{N}_2\text{O}} \\ T_{\text{surface}} \\ P_{\text{cloud}} \\ \tau_{\text{cloud}} \end{bmatrix} = \mathbf{M} \begin{bmatrix} Z_{\text{H}_2\text{O}} \\ Z_{\text{HDO}} \\ Z_{\text{CH}_4} \\ Z_{\text{N}_2\text{O}} \\ T_{\text{surface}} \\ P_{\text{cloud}} \\ \tau_{\text{cloud}} \end{bmatrix} \quad (5)$$

where the vectors  $\mathbf{x}$  are on a 67 level pressure grid ranging from 1000 hPa to 0.1 hPa (Worden et al., 2004),  $T_{\text{surface}}$  is the surface temperature,  $P_{\text{cloud}}$  is the cloud top pressure, and  $\tau_{\text{cloud}}$  is the cloud effective optical as a function of frequency (e.g., Kulawik et al., 2006b; Eldering et al., 2007). As discussed earlier, the atmospheric species are retrieved on a subset of the 67 level pressure grid used in the TES forward model; this effective hard constraint is described by the mapping matrix “ $\mathbf{M}$ ” and the retrieval levels “ $z$ ” in Eq. 1) (Worden et al., 2004; Bowman et al., 2006) and must formally be included in the error analysis; however, for the sake of brevity we exclude this term in subsequent equations.

## 3.3 Constraints

A primary objective for these new TES retrievals is to increase the vertical resolution and information content of methane,  $\text{H}_2\text{O}$ , and the  $\text{HDO}/\text{H}_2\text{O}$  ratio in the lower troposphere. The added spectral data cannot by themselves allow for these objectives to be met because the choice of regularization in the previous versions of the TES data limited sensitivity at specific altitudes in order to reduce impacts of non-linearity on the retrieval due to low sensitivity. Consequently, we need to change both the hard constraint (or retrieval levels and mapping matrices) as shown by Eq. (5) and the soft

Title Page

Abstract

Introduction

Conclusions

References

Tables

Figures

◀

▶

◀

▶

Back

Close

Full Screen / Esc

Printer-friendly Version

Interactive Discussion



---

**Profiles of CH<sub>4</sub>, HDO,  
H<sub>2</sub>O, and N<sub>2</sub>O**J. Worden et al.

---

[Title Page](#)[Abstract](#)[Introduction](#)[Conclusions](#)[References](#)[Tables](#)[Figures](#)[◀](#)[▶](#)[◀](#)[▶](#)[Back](#)[Close](#)[Full Screen / Esc](#)[Printer-friendly Version](#)[Interactive Discussion](#)

constraints (constraint matrix shown in Eq. 2). Previously, the retrieval levels ( $z$ ) for H<sub>2</sub>O and HDO in the lower troposphere (surface to 500 hPa) tropospheric were defined as every other forward model level ( $x$ ); with the mapping matrix using linear in (log) pressure and (log) mixing ratio to interpolate between retrieval levels and forward model levels. The new retrieval levels in the lower troposphere now have a one-to-one mapping with the TES forward model levels for H<sub>2</sub>O and HDO. For methane, the retrieval level density has been increased from every 3rd level to every 2nd forward model level for CH<sub>4</sub>. The constraints were selected based on the altitude-dependent Tikhonov constraints as described in Kulawik et al. (2006a).

In optimal estimation, the constraint matrix is typically calculated from the known a priori statistics of the atmosphere (e.g., Rodgers, 2000). These statistics are most easily generated from global chemical or climate models. However, covariances from these models are not typically invertible, can vary from model to model, and may not replicate actual correlations for molecules such as HDO that are not well observed. We therefore modify the derived correlations from the models by the sensitivity of the radiances to each geophysical parameter (e.g., Kulawik et al., 2006a) or from insight derived from more recent data sets such as water vapor isotope data at the Mauna Loa observatory (Worden et al., 2011). For the new TES retrievals of H<sub>2</sub>O, HDO, and CH<sub>4</sub>, the correlation length scales in the constraint matrices (not shown as the larger variance and negative correlations make these plots difficult to generate) have been reduced between the mixing layer (typically surface to 825 hPa) and lower troposphere to reflect conclusions drawn from recent in situ and satellite based observations of these constituents (e.g., Frankenberg et al., 2005, 2009; Worden et al., 2011; Pickett-Heaps et al., 2011; Noone et al., 2011).

#### 4 Comparison of previous (version 6.0 or less) and new profile retrievals

The effective vertical resolution (as characterized by the averaging kernels) and the calculated uncertainties of these new data are compared to the earlier retrieval approach.

We also compare old versus new retrievals for the altitude region in which the vertical sensitivities overlap. However, validation of the new data sets in altitude regions where the sensitivity has been improved will be published in subsequent papers.

## 4.1 H<sub>2</sub>O

5 Figure 3a shows the averaging kernels for the new and old H<sub>2</sub>O retrievals for a tropical ocean case and Fig. 3b shows the square-root of the diagonals of the corresponding a priori, a posteriori error, and observation covariances. As discussed earlier, the averaging kernels (or rows of the averaging kernel matrix) describe the sensitivity of estimate to the true state, e.g.:  $\mathbf{A} = \frac{\partial \hat{x}}{\partial x}$  where  $\hat{x}$  is the estimate and  $x$  is the true state.  
10 As shown in Eq. (1), in the absence of uncertainties, the estimate is related to the true state via the a priori constraint and the averaging kernel matrix (Rodgers, 2000):

$$\hat{x} = x_a + \mathbf{A}(x - x_a) \quad (6)$$

An “ideal” averaging kernel would approach the identity matrix. The rows would exhibit narrowly defined peaks, with the peak value of each row located at the pressure of the retrieval level assigned to that row. In the absence of error, the retrieved estimate would then approach the true state. Figure 3a shows that the H<sub>2</sub>O averaging kernels have narrower vertical extent and are more distinct for the new retrievals, while Fig. 3b shows that the uncertainties for the new retrieval are overall reduced, except near pressures around 700 hPa for this retrieval.

20 Figure 4 shows the RMS difference and mean bias between the new (TES Version 6.1) and older (TES Version 6.0) H<sub>2</sub>O profile retrievals. The RMS difference is consistent with the random uncertainties in the estimate as seen in the previous figure. In addition, the bias between the versions is effectively zero except at the lowermost pressures where the sensitivity has increased in the tropics through the mid-latitudes.

Title Page

Abstract

Introduction

Conclusions

References

Tables

Figures

◀

▶

◀

▶

Back

Close

Full Screen / Esc

Printer-friendly Version

Interactive Discussion



## 4.2 HDO/H<sub>2</sub>O ratio covariances and mapping

The TES HDO and H<sub>2</sub>O retrieval approach is designed to reduce the uncertainties in the HDO/H<sub>2</sub>O ratio estimate as opposed to HDO or H<sub>2</sub>O separately (e.g., Worden et al., 2006; Schneider et al., 2006). Consequently, the constraint used to regularize this retrieval is based on an a priori covariance that characterizes the HDO/H<sub>2</sub>O ratio variability, under the assumption that HDO and H<sub>2</sub>O are jointly estimated, i.e.:

$$\mathbf{S}_a = \begin{bmatrix} \mathbf{S}_a^H + \mathbf{S}_a^R & \mathbf{S}_a^H \\ \mathbf{S}_a^H & \mathbf{S}_a^H \end{bmatrix} \quad (7)$$

where  $\mathbf{S}_a^H$  is the a priori covariance for H<sub>2</sub>O and  $\mathbf{S}_a^R$  is the a priori covariance for the HDO/H<sub>2</sub>O ratio. The a priori covariance for water,  $\mathbf{S}_H$ , is constructed using statistics from the MOZART (e.g., Brasseur et al., 1998; Horowitz et al., 2003) model but scaled to the expected uncertainty of NCEP water content predictions (Worden et al., 2004). The a priori statistics for  $\mathbf{S}_R$  are originally based on a version of the National Center for Atmospheric Research (NCAR) Community Atmosphere Model (CAM) (e.g., Collins et al., 2004) that has been modified to predict the isotopic composition of water using the approach developed by Noone and Simmonds (2002). However, we now adjust  $\mathbf{S}_R$  to reduce correlations between the PBL and the lower troposphere and increase the variance in the boundary layer and free troposphere, consistent with recent observations of the PBL and free troposphere in the subtropics at Mauna Loa (Worden et al., 2010; Noone et al., 2011).

There is no unique averaging kernel for the estimate of the HDO/H<sub>2</sub>O ratio (Worden et al., 2006). However, the HDO estimate will always be sensitive to the same air parcels as the H<sub>2</sub>O estimate. Consequently, the HDO averaging kernel best describes the vertical sensitivity for the HDO/H<sub>2</sub>O estimate characteristics. The HDO averaging kernel matrix and square root of the diagonal of the HDO/H<sub>2</sub>O error covariances are shown in Fig. 5 for the same tropical case shown in Fig. 3. The degrees-of-freedom for signal (DOFS) for the HDO/H<sub>2</sub>O estimate has greatly increased but there

Title Page

Abstract

Introduction

Conclusions

References

Tables

Figures

◀

▶

◀

▶

Back

Close

Full Screen / Esc

Printer-friendly Version

Interactive Discussion



is a net increase in the error in the boundary layer due to temperature and noise of approximately 3%. On the other hand, the total error for the HDO/H<sub>2</sub>O ratio in the free troposphere has decreased because the increased vertical resolution reduces the smoothing error.

#### 4.2.1 Global comparison of version 6.1 and previous HDO/H<sub>2</sub>O estimates

TES products prior to version 6 have been validated in the lower troposphere by comparing TES estimates to in situ measurements of HDO and H<sub>2</sub>O at the Mauna Loa observatory (Worden et al., 2011). While there is insufficient data to provide direct validation of the profiles of the new TES HDO/H<sub>2</sub>O estimates in the free troposphere, we can compare the new TES estimates in the lower troposphere to the older estimates in the lower troposphere where the sensitivities overlap. This comparison is shown in Fig. 6. The first panel of Fig. 6 shows the latitudinal distribution of  $\delta - D$  between the old and new HDO/H<sub>2</sub>O estimates for the vertical range between 825 and 500 hPa for all scenes in which the degrees of freedom for signal (or trace of the averaging kernel) are larger than 1.0. For a log-based retrieval, the DOF is a good metric for retrieval sensitivity as it indicates how well an ensemble of estimates captures the range of variability of the true distribution. For example, if the DOFS is 0.5 for some altitude range than that means a distribution of estimates, averaged over that altitude, could be expected to capture half the natural variability of the true distribution. The data in the top panel of Fig. 6 are taken from one TES global survey in July 2005. Note that the HDO/H<sub>2</sub>O ratio is given in parts per thousand relative to the isotopic composition of ocean water (per mil) or  $\delta - D = 1000(R/R_{\text{std}} - 1)$ , where  $R$  is the HDO/H<sub>2</sub>O mole ratio and  $R_{\text{std}} = 3.11 \times 10^{-4}$  is 2 times the isotope ratio of the Vienna Standard mean Ocean water reference for the D/H. As can be seen in this figure, there are many more retrievals at higher latitudes that meet this DOF's criteria as the sensitivity of the new retrievals have improved. The bottom panel shows the difference between the new and old estimates, averaged between 825 and 500 hPa, for all retrievals with DOFS greater than 1.0 in order to reduce uncertainty in the comparison due to differences in the

Title Page

Abstract

Introduction

Conclusions

References

Tables

Figures

◀

▶

◀

▶

Back

Close

Full Screen / Esc

Printer-friendly Version

Interactive Discussion



retrieval sensitivity. Figure 6 shows that the RMS difference between the two versions is consistent with the expected uncertainties of the HDO/H<sub>2</sub>O estimate; however the bias has changed by 7.5‰, likely because of the increased number of HDO and H<sub>2</sub>O lines used for the new estimate.

#### 5 4.2.2 Global estimates of the HDO/H<sub>2</sub>O ratio for July 2006

A limited number of TES global surveys have been processed with the new retrieval approach and the results are shown in Fig. 7. The top panel of Fig. 7 shows the HDO/H<sub>2</sub>O ratio for the altitudes approximately corresponding to the free troposphere (800 to 300 hPa) and the bottom panel shows the HDO/H<sub>2</sub>O ratio for altitudes that approximately corresponds to the boundary layer (surface to 800 hPa) regions. Values of the HDO/H<sub>2</sub>O ratio are given in per mil and have been corrected for the estimated TES bias discussed in the previous section (Worden et al., 2011). Only data in which the DOFS for the HDO estimate is larger than 1 and where the cloud optical depth is less than 0.4 are shown. Note that even though the DOFS can be approximately one, the HDO/H<sub>2</sub>O profile can still distinguish boundary layer variability from free tropospheric variability of the HDO/H<sub>2</sub>O ratio as long as the peak values of the averaging kernels (rows of averaging kernel matrix) in these regions are separated; this condition should be met for most clear-sky regions. In the boundary layer above the ocean, mean values of the HDO/H<sub>2</sub>O ratio are approximately -74‰ with an RMS variance of 37‰, consistent with the 3% uncertainty shown for the tropical case in Fig. 5b (for isotopic values near 0.0 a 3% uncertainty corresponds to 30‰ uncertainty). The -74‰ mean value for the mean tropical ocean boundary layer is consistent with in situ measurements for boundary layer water vapor (e.g., Lawrence et al., 2004; Galewsky et al., 2007; Worden et al., 2011) and therefore suggests that the bias correction calculated for the previous TES HDO/H<sub>2</sub>O estimates are applicable for these data.

Title Page

Abstract

Introduction

Conclusions

References

Tables

Figures

◀

▶

◀

▶

Back

Close

Full Screen / Esc

Printer-friendly Version

Interactive Discussion



### 4.3 CH<sub>4</sub> profiles

In this section we describe the changes in the vertical resolution and error characteristics of the new TES CH<sub>4</sub> methane retrievals as well as biases in the profiles. We then discuss approaches for correcting or accounting for this bias including averaging, or correcting the methane estimate using the co-retrieved N<sub>2</sub>O estimate, a temperature based correction is probably also needed. However subsequent analysis using independent methane data sets will be needed in order to determine the optimal approach for this bias correction.

#### 4.3.1 Vertical sensitivity and resolution

Figure 8a and b shows the averaging kernels for the previous and new CH<sub>4</sub> estimate for the same tropical case shown in Figs. 3 and 5 for H<sub>2</sub>O and HDO. The new CH<sub>4</sub> methane profile estimates generally show increased sensitivity to the lower and mid troposphere between 825 and 450 hPa. In addition, the averaging kernels generally peak around 650 hPa and 300 hPa indicating that methane variations at these altitudes can theoretically be distinguished from one another provided the vertical variations are larger than the expected uncertainties. This increased sensitivity to the lower and middle troposphere is due to use of the methane lines around 1230 cm<sup>-1</sup> (Fig. 2a) because the lower optical thickness at these wavelengths allows for greater sensitivity to lower tropospheric methane; Fig. 9 shows the DOF's for the new and older methane retrievals. Typically there are about 0.5 DOFS more for the new retrieval than the old with the increased sensitivity in the middle / lower troposphere.

#### 4.3.2 CH<sub>4</sub> error characteristics

Error characteristics for the TES methane estimate using the radiance from the tropical scene shown in Fig. 5 are presented in the left panel of Fig. 10. For the TES methane retrieval we assume an a priori 5 % uncertainty in methane but with significant (>50 %)

Title Page

Abstract

Introduction

Conclusions

References

Tables

Figures

◀

▶

◀

▶

Back

Close

Full Screen / Esc

Printer-friendly Version

Interactive Discussion



cross-correlations between adjacent levels (not shown) because methane is a well mixed gas in the free troposphere (e.g., Fung et al., 1991; Wofsy et al., 2011). For this case, the observation error describes the estimated error from noise and from co-retrieved geophysical parameters such as H<sub>2</sub>O, HDO, surface temperature, and clouds, as well as parameters estimated in a previous step such as O<sub>3</sub> and CO<sub>2</sub>. Because temperature is retrieved from a previous step using the CO<sub>2</sub>v2 band around 700 cm<sup>-1</sup>, its error estimate is shown separately. As can be seen in this figure, uncertainty due to temperature is the largest component of the methane retrieval error budget in the lower/middle troposphere.

### 4.3.3 Global distribution of TES observed methane and biases

Because of the long life-time of approximately nine years for methane (e.g., Frankenberg et al., 2005) we would expect that methane should be a vertically well mixed gas in the free troposphere (e.g., Wofsy et al., 2011; Pickett-Heaps et al., 2011) but showing a latitudinal gradient that depends on inter-hemispheric mixing, the preponderance of northern hemispheric methane sources relative to the Southern Hemisphere, and the distribution of OH which is the primary sink for CH<sub>4</sub> (e.g., Fung et al., 1991). Consequently, it is reasonable to show a two-dimensional figure of the vertical profile of methane as a function of latitude, averaged over all longitudes as well as ocean and land scenes, in order to infer any vertical biases in the TES methane estimates. Figure 11 shows the TES estimated vertical distribution of methane as a function of latitude for all data taken during July 2006. A feature of this distribution is that methane is biased high in the upper troposphere and lower stratosphere. This upper tropospheric bias was suspected for previous TES methane estimates that were only sensitive to methane in the upper troposphere (Payne et al., 2009). Based on these observations we suspect that either a systematic bias in temperature is affecting the TES methane estimates, or that temperature dependent uncertainties in the methane spectroscopic line strengths are affecting these estimates. Another possibility is that the bias is due to anti-correlations of the estimated upper tropospheric methane with the middle/lower

Title Page

Abstract

Introduction

Conclusions

References

Tables

Figures

◀

▶

◀

▶

Back

Close

Full Screen / Esc

Printer-friendly Version

Interactive Discussion



**Profiles of CH<sub>4</sub>, HDO,  
H<sub>2</sub>O, and N<sub>2</sub>O**

J. Worden et al.

[Title Page](#)[Abstract](#)[Introduction](#)[Conclusions](#)[References](#)[Tables](#)[Figures](#)[◀](#)[▶](#)[◀](#)[▶](#)[Back](#)[Close](#)[Full Screen / Esc](#)[Printer-friendly Version](#)[Interactive Discussion](#)

5 tropospheric methane estimate as shown in the methane averaging kernels (right panel Fig. 8); in order to determine if this anti-correlation could account for some of this bias we show a global map of the middle troposphere at 618 hPa versus a global map using an information based averaging approach described by Payne et al. (2007) which maps  
10 each profile to one or two levels that best represent the altitude where the estimate has the most sensitivity; this approach limits the impact of the a priori on an average because the averaging kernel approaches unity for the re-mapped estimate. For the approach using the Payne et al. (2007) algorithm we only choose methane estimates for which the pressure of the re-mapped (or information averaged) estimate is greater  
15 than 450 hPa. Figure 12 (bottom panel) shows global methane estimate from TES for July 2006 for re-mapped estimate. The average pressure for this re-mapped estimate is approximately 500 hPa. Figure 12 (top panel) shows the TES global methane estimate for July 2006 for the 562 hPa pressure level. While both maps show an expected latitudinal gradient, the map using the methane estimate from the TES 562 hPa pressure level shows un-physically high methane at around  $-50$  degrees relative to the tropics; however, the map derived from the averaged values shows a more realistic latitudinal gradient as compared to previous measurements (e.g., Frankenberg et al.,  
20 2006). This result suggests that the anti-correlations in the profile estimate accounts for part of this bias. Future comparisons between the TES data and independent methane measurements will be needed to further characterize this bias so that this data can be used for understanding the global methane cycle. In the next section, we describe an additional approach (e.g., Razavi et al., 2009) in which we correct the methane estimate using co-retrieved N<sub>2</sub>O estimates. The theoretical calculation of errors using this approach is promising but depends on accurate a priori knowledge of the tropospheric and stratospheric N<sub>2</sub>O distribution.  
25

#### 4.3.4 Methane profile correction using N<sub>2</sub>O estimate

In this section we describe an approach for reducing errors in the methane estimates using the co-retrieved N<sub>2</sub>O estimates. We show that while correcting the methane

## Profiles of CH<sub>4</sub>, HDO, H<sub>2</sub>O, and N<sub>2</sub>O

J. Worden et al.

Title Page

Abstract

Introduction

Conclusions

References

Tables

Figures

◀

▶

◀

▶

Back

Close

Full Screen / Esc

Printer-friendly Version

Interactive Discussion



estimates with N<sub>2</sub>O shows promise in reducing bias errors, it requires estimates of the a priori distribution of N<sub>2</sub>O in which the uncertainties in this distribution are much smaller than the uncertainties in CH<sub>4</sub>. For the current TES estimates, this requirement is not achieved; however, we are looking into obtaining improved a priori distributions of N<sub>2</sub>O that will meet these requirements.

Although N<sub>2</sub>O varies much less than CH<sub>4</sub> in the troposphere, the top-of-atmosphere radiance is affected by N<sub>2</sub>O and CH<sub>4</sub> nearly identically at 8 microns as shown by their normalized column Jacobians in Fig. 2a. We assume here that the tropospheric N<sub>2</sub>O profile is well represented by the a priori profile, and that deviations in the retrieved N<sub>2</sub>O from the prior are a result of systematic error. Interference error from temperature, clouds, and emissivity should therefore affect both CH<sub>4</sub> and N<sub>2</sub>O very similarly, and correction of CH<sub>4</sub> by N<sub>2</sub>O should therefore reduce the CH<sub>4</sub> errors. This correction takes the following form:

$$\hat{x}_c^{\text{adj}} = \hat{x}_c - \hat{x}_n + \hat{x}_n^a, \quad (8)$$

where  $x_c$  is the estimate for (log) methane,  $x_n$  is the (log) estimate for N<sub>2</sub>O, and the adj superscript means “adjusted” or corrected. Because this is simply the ratio of two numbers (for a logarithm) modified by an a priori constraint we can use the same derivation for the errors in the HDO/H<sub>2</sub>O estimate as described in Worden et al. (2006) or Schneider et al. (2006). For the methane estimate this leads to:

$$\hat{x}_c^{\text{adj}} = x_c^a + (\mathbf{A}_{cc} - \mathbf{A}_{nc})(x_c - x_c^a) - (\mathbf{A}_{nn} - \mathbf{A}_{cn})(x_n - x_n^a) + \sum_j (\mathbf{A}_{cj} - \mathbf{A}_{nj})(x_j - x_j^a) + \mathbf{G}_R \mathbf{m} + \mathbf{G}_R \sum_i \mathbf{K}_i^b (b_i - b_i^a) \quad (9)$$

Note that the full averaging kernel contains entries for the joint estimate of CH<sub>4</sub>, N<sub>2</sub>O, H<sub>2</sub>O, HDO, surface temperature, clouds and emissivity. The  $\mathbf{A}_{cc}$  term is the component of this averaging kernel that just corresponds to the (log) CH<sub>4</sub> estimate. The  $\mathbf{A}_{cn}$  term is the component of the averaging kernel that represents how the (log) N<sub>2</sub>O estimate

## Profiles of CH<sub>4</sub>, HDO, H<sub>2</sub>O, and N<sub>2</sub>O

J. Worden et al.

Title Page

Abstract

Introduction

Conclusions

References

Tables

Figures

◀

▶

◀

▶

Back

Close

Full Screen / Esc

Printer-friendly Version

Interactive Discussion



affects the jointly retrieved (log) methane estimate (using indices “n” for N<sub>2</sub>O and “c” for CH<sub>4</sub>). The term  $\mathbf{G}_r$  is the gain matrix for the CH<sub>4</sub> methane part of the retrieval vector minus that of the N<sub>2</sub>O part of the retrieval vector ( $\mathbf{G}_r = \mathbf{G}_c - \mathbf{G}_n$ ). The term  $\mathbf{G}_R \mathbf{m}$  is the impact of measurement noise on the estimate. The index “j” is for jointly retrieved parameters such as H<sub>2</sub>O or HDO and the index  $i$  refers to un-retrieved parameters such as atmospheric temperature, spectroscopy or calibration. Taking the expectation of the adjusted CH<sub>4</sub> methane estimate minus the true CH<sub>4</sub> methane distribution (e.g., Bowman et al., 2006) yields the second order statistics for Eq. (9):

$$\mathbf{S}_{\bar{c}} = (\mathbf{A}_{cc} - \mathbf{A}_{nc} - \mathbf{I})\mathbf{S}_{cc}(\mathbf{A}_{cc} - \mathbf{A}_{nc} - \mathbf{I})^T + (\mathbf{A}_{nn} - \mathbf{A}_{cn} - \mathbf{I})\mathbf{S}_{nn}(\mathbf{A}_{nn} - \mathbf{A}_{cn} - \mathbf{I})^T + \sum_j (\mathbf{A}_{cj} - \mathbf{A}_{nj})\mathbf{S}_{jj}(\mathbf{A}_{cj} - \mathbf{A}_{nj})^T + \mathbf{G}_R \mathbf{S}_m \mathbf{G}_R^T + \mathbf{G}_R \left( \sum_i \mathbf{K}_i \mathbf{S}_i^j \mathbf{K}_i^T \right) \mathbf{G}_R^T \quad (10)$$

Results show that each term of the cross averaging kernels for the N<sub>2</sub>O and CH<sub>4</sub> estimates are small relative to the averaging kernels for N<sub>2</sub>O and CH<sub>4</sub> ( $\mathbf{A}_{nc} \ll \mathbf{A}_{cc}$  and  $\mathbf{A}_{cn} \ll \mathbf{A}_{nn}$ ); consequently we can ignore the cross averaging kernels. Under the assumption that the variability of N<sub>2</sub>O in the atmosphere is much smaller than the variability of CH<sub>4</sub> (Wofsy et al., 2011) in the atmosphere we can ignore the term associated with  $\mathbf{S}_{nn}$ . This leads to an error estimate for methane, corrected by the N<sub>2</sub>O estimate of:

$$\mathbf{S}_{\bar{c}} = (\mathbf{A}_{cc} - \mathbf{I})\mathbf{S}_{cc}(\mathbf{A}_{cc} - \mathbf{I})^T + \sum_j (\mathbf{A}_{cj} - \mathbf{A}_{nj})\mathbf{S}_{jj}(\mathbf{A}_{cj} - \mathbf{A}_{nj})^T + \mathbf{G}_R \mathbf{S}_m \mathbf{G}_R^T + \mathbf{G}_R \left( \sum_i \mathbf{K}_i \mathbf{S}_i^j \mathbf{K}_i^T \right) \mathbf{G}_R^T \quad (11)$$

The right panel of Fig. 10 shows the error budget for these terms. While the observation error (error due to noise and from jointly estimated parameters such as H<sub>2</sub>O, clouds, etc.) and smoothing error is approximately the same for CH<sub>4</sub> with and without the N<sub>2</sub>O correction, the temperature error is much smaller after applying the N<sub>2</sub>O correction, providing evidence of the reduction in errors due to parameters that are not retrieved. We would also expect this same approach to work for the bias error described in Eq. (9).

[Title Page](#)[Abstract](#)[Introduction](#)[Conclusions](#)[References](#)[Tables](#)[Figures](#)[◀](#)[▶](#)[◀](#)[▶](#)[Back](#)[Close](#)[Full Screen / Esc](#)[Printer-friendly Version](#)[Interactive Discussion](#)

For example, Fig. 13 shows the two-dimensional (latitude versus altitude) distribution of TES estimated CH<sub>4</sub> methane. As compared to Fig. 11, the bias in the upper troposphere is greatly reduced. However, there are now significant “jumps” in the latitudinal variability of the methane distribution that correspond to the discretization of the N<sub>2</sub>O a priori distribution used for these estimates (Fig. 14). As shown in Eq. (9), there is a term that depends on the difference between the true N<sub>2</sub>O distribution and the a priori distribution; this term must be effectively zero in order for this correction to be more robust.

## 5 Summary

This manuscript documents improvements to the Aura TES profile estimates of H<sub>2</sub>O, HDO/H<sub>2</sub>O, and CH<sub>4</sub> by using a joint retrieval over a wide spectral range. In general, the vertical resolution of H<sub>2</sub>O has increased in the lower troposphere with improved capability to distinguish between boundary layer variability of H<sub>2</sub>O and that of the free troposphere. Previous (version 5.0 or less) retrievals could not profile the HDO/H<sub>2</sub>O ratio but were instead sensitive to an average over the lower troposphere between 550 and 825 hPa. New TES estimates of the HDO/H<sub>2</sub>O profile can now distinguish between the boundary layer/lower troposphere and the middle troposphere around 550 hPa with uncertainties of approximately 30% for the HDO/H<sub>2</sub>O ratio in the boundary layer. We show that the new and old estimates for the HDO/H<sub>2</sub>O estimates are consistent within the expected uncertainties in the regions where the vertical sensitivity overlaps.

The new TES methane estimates are now sensitive to methane variability from approximately 800 hPa to 200 hPa whereas previous TES retrievals were only sensitive to methane in the mid- to upper troposphere. However, there is clearly a bias in the upper tropospheric methane that must be better characterized with respect to other parameters that affect the TES methane estimates before this profile information can be used. The effect of this bias on the latitudinal distribution of the TES methane profiles is mitigated if the profiles are averaged to account for the vertical distribution



**Profiles of CH<sub>4</sub>, HDO,  
H<sub>2</sub>O, and N<sub>2</sub>O**

J. Worden et al.

[Title Page](#)[Abstract](#)[Introduction](#)[Conclusions](#)[References](#)[Tables](#)[Figures](#)[◀](#)[▶](#)[◀](#)[▶](#)[Back](#)[Close](#)[Full Screen / Esc](#)[Printer-friendly Version](#)[Interactive Discussion](#)

Brown, D., Worden, J., and Noone, D.: Comparison of atmospheric hydrology over convective continental regions using water vapor isotope measurements from space, *J. Geophys. Res.-Atmos.*, 113, D15124, doi:10.1029/2007JD009676, 2008.

5 Clough, S. A., Shephard, M. W., Worden, J., Brown, P. D., Worden, H. M., Luo, M., Rodgers, C. D., Rinsland, C. P., Goldman, A., Brown, L., Kulawik, S. S., Eldering, A., Lampel, M., Osterman, G., Beer, R., Bowman, K., Cady-Pereira, K. E., and Mlawer, E. J.: Forward model and Jacobians for Tropospheric Emission Spectrometer retrievals, *IEEE Transactions on Geoscience and Remote Sensing*, 44, 1308–1323, 2006.

Dessler, A. E. and Minschwaner, K.: An analysis of the regulation of tropical tropospheric water vapor, *J. Geophys. Res.-Atmos.*, 112, D10120, doi:10.1029/2006JD007683, 2007.

10 Dudhia, A., Jay, V. L., and Rodgers, C. D.: Microwindow selection for high-spectral-resolution sounders, *Appl. Optics*, 41, 3665–3673, 2002.

Echle, G., von Clarmann, T., Dudhia, A., Flaud, J. M., Funke, B., Glatthor, N., Kerridge, B., Lopez-Puertas, M., Martin-Torres, F. J., and Stiller, G. P.: Optimized spectral microwindows for data analysis of the Michelson Interferometer for Passive Atmospheric Sounding on the environmental satellite, *Appl. Optics*, 39, 5531–5540, 2000.

Frankenberg, C., Meirink, J. F., van Weele, M., Platt, U., and Wagner, T.: Assessing Methane Emissions from Global Space-Borne Observations, *Science*, 308, 1010–1014, doi:10.1126/science.1106644, 2005.

20 Frankenberg, C., Meirink, J. F., Bergamaschi, P., Goede, A. P. H., Heimann, M., Korner, S., Platt, U., van Weele, M., and Wagner, T.: Satellite cartography of atmospheric methane from SCIAMACHY on board ENVISAT: Analysis of the years 2003 and 2004, *J. Geophys. Res.-Atmos.*, 111, D07303, doi:10.1029/2005JD006235, 2006.

25 Frankenberg, C., Yoshimura, K., Warneke, T., Aben, I., Butz, A., Deutscher, N., Griffith, D., Hase, F., Notholt, J., Schneider, M., Schrijver, H., and Rockmann, T.: Dynamic Processes Governing Lower-Tropospheric HDO/H<sub>2</sub>O Ratios as Observed from Space and Ground, *Science*, 325, 1374–1377, 2009.

Fung, I., John, J., Lerner, J., Matthews, E., Prather, M., Steele, L. P., and Fraser, P. J.: 3-Dimensional Model Synthesis of the Global Methane Cycle, *J. Geophys. Res.-Atmos.*, 96, 13033–13065, 1991.

30 Herbin, H., Hurtmans, D., Clerbaux, C., Clarisse, L., and Coheur, P.-F.: H<sub>2</sub><sup>16</sup>O and HDO measurements with IASI/MetOp, *Atmos. Chem. Phys.*, 9, 9433–9447, doi:10.5194/acp-9-9433-2009, 2009.

**Profiles of CH<sub>4</sub>, HDO,  
H<sub>2</sub>O, and N<sub>2</sub>O**

J. Worden et al.

Title Page

Abstract

Introduction

Conclusions

References

Tables

Figures

◀

▶

◀

▶

Back

Close

Full Screen / Esc

Printer-friendly Version

Interactive Discussion



- Jiang, X., Li, Q. B., Liang, M. C., Shia, R. L., Chahine, M. T., Olsen, E. T., Chen, L. L., and Yung, Y. L.: Simulation of upper tropospheric CO(2) from chemistry and transport models, *Global Biogeochem. Cycles*, 22, GB4025, doi:10.1029/2007GB003049, 2008.
- 5 Kuai, L., Natraj, V., Shia, R. L., Miller, C. and Yung, Y. L.: Channel selection using information content analysis: A case study of CO(2) retrieval from near infrared measurements, *Journal of Quantitative Spectroscopy & Radiative Transfer*, 111, 1296-1304, 2010.
- Kuang, Z. M., Toon, G. C., Wennberg, P. O., and Yung, Y. L.: Measured HDO/H<sub>2</sub>O ratios across the tropical tropopause, *Geophys. Res. Lett.*, 30, 1372, doi:10.1029/2003GL017023, 2003.
- 10 Kulawik, S. S., Osterman, G., Jones, D. B. A., and Bowman, K. W.: Calculation of altitude-dependent Tikhonov constraints for TES nadir retrievals, *IEEE Transactions on Geoscience and Remote Sensing*, 44, 1334–1342, 2006a.
- Kulawik, S. S., Worden, J., Eldering, A., Bowman, K., Gunson, M., Osterman, G. B., Zhang, L., Clough, S. A., Shephard, M. W., and Beer, R.: Implementation of cloud paper retrievals for Tropospheric Emission Spectrometer (TES) atmospheric retrievals: part 1. Description and characterization of errors on trace gas retrievals, *J. Geophys. Res.-Atmos.*, 111, D24204, doi:10.1029/2005JD006733, 2006b.
- 15 Lee, J. E., Pierrehumbert, R., Swann, A., and Lintner, B. R.: Sensitivity of stable water isotopic values to convective parameterization schemes, *Geophys. Res. Lett.*, 36, L23801, doi:10.1029/2009GL040880, 2009.
- 20 Li, K. F., Tian, B. J., Waliser, D. E., and Yung, Y. L.: Tropical mid-tropospheric CO(2) variability driven by the Madden-Julian oscillation, *Proc. Natl. Acad. Sci. USA*, 107, 19171–19175, 2010.
- Nassar, R., Bernath, P. F., Boone, C. D., Gettelman, A., McLeod, S. D., and Rinsland, C. P.: Variability in HDO/H<sub>2</sub>O abundance ratios in the tropical tropopause layer, *J. Geophys. Res.*, 112, D21305, doi:10.1029/2007JD008417, 2007.
- 25 Nassar, R., Jones, D. B. A., Kulawik, S. S., Worden, J. R., Bowman, K. W., Andres, R. J., Suntharalingam, P., Chen, J. M., Brenninkmeijer, C. A. M., Schuck, T. J., Conway, T. J., and Worthy, D. E.: Inverse modeling of CO<sub>2</sub> sources and sinks using satellite observations of CO<sub>2</sub> from TES and surface flask measurements, *Atmos. Chem. Phys.*, 11, 6029–6047, doi:10.5194/acp-11-6029-2011, 2011.
- 30 Noone, D.: Measurements of water vapor isotope ratio with humidity to deduce atmospheric moistening and dehydration in the tropical mid-troposphere, *J. Climate*, in review, 2011.
- Noone, D. and Simmonds, I.: Associations between d18O of water and climate parameters in

---

**Profiles of CH<sub>4</sub>, HDO,  
H<sub>2</sub>O, and N<sub>2</sub>O**


---

J. Worden et al.

Title Page

Abstract

Introduction

Conclusions

References

Tables

Figures

◀

▶

◀

▶

Back

Close

Full Screen / Esc

Printer-friendly Version

Interactive Discussion



a simulation of atmospheric circulation for 1979–1995, *J. Climate*, 15, 3150–3169, 2002.

Noone, D., Galewsky, J., Sharp, Z., Worden, J., Barnes, J., Baer, D., Bailey, A., Brown, D., Christensen, L., Crosson, E., Dong, F., Hurley, J., Johnson, L., Strong, M., Toohey, D., Van Pelt, A., and Wright, J.: Properties of air mass mixing and humidity in the subtropics from measurements of the D/H isotope ratio of water vapor at the Mauna Loa Observatory, *J. Geophys. Res.-A*, in review, 2011.

Payne, V. H., Noone, D., Dudhia, A., Piccolo, C., and Grainger, R. G.: Global satellite measurements of HDO and implications for understanding the transport of water vapour into the stratosphere, *Q. J. Roy. Meteorol. Soc.*, 133, 1459–1471, 2007.

Payne, V. H., Clough, S. A., Shephard, M. W., Nassar, R., and Logan, J. A.: Information-centered representation of retrievals with limited degrees of freedom for signal: Application to methane from the Tropospheric Emission Spectrometer, *J. Geophys. Res.*, 114, D10307, doi:10.1029/2008JD010155, 2009.

Pickett-Heaps, C. A., Jacob, D. J., Wecht, K. J., Kort, E. A., Wofsy, S. C., Diskin, G. S., Worthy, D. E. J., Kaplan, J. O., Bey, I., and Drevet, J.: Magnitude and seasonality of wetland methane emissions from the Hudson Bay Lowlands (Canada), *Atmos. Chem. Phys.*, 11, 3773–3779, doi:10.5194/acp-11-3773-2011, 2011.

Querino, C. A. S., Smeets, C. J. P. P., Vigano, I., Holzinger, R., Moura, V., Gatti, L. V., Martinewski, A., Manzi, A. O., de Araújo, A. C., and Röckmann, T.: Methane flux, vertical gradient and mixing ratio measurements in a tropical forest, *Atmos. Chem. Phys.*, 11, 7943–7953, doi:10.5194/acp-11-7943-2011, 2011.

Razavi, A., Clerbaux, C., Wespes, C., Clarisse, L., Hurtmans, D., Payan, S., Camy-Peyret, C., and Coheur, P. F.: Characterization of methane retrievals from the IASI space-borne sounder, *Atmos. Chem. Phys.*, 9, 7889–7899, doi:10.5194/acp-9-7889-2009, 2009.

Read, W. G., Schwartz, M. J., Lambert, A., Su, H., Livesey, N. J., Daffer, W. H., and Boone, C. D.: The roles of convection, extratropical mixing, and in-situ freeze-drying in the Tropical Tropopause Layer, *Atmos. Chem. Phys.*, 8, 6051–6067, doi:10.5194/acp-8-6051-2008, 2008.

Risi, C., Bony, S., and Vimeux, F.: Influence of convective processes on the isotopic composition (delta O-18 and delta D) of precipitation and water vapor in the tropics: 2. Physical interpretation of the amount effect, *J. Geophys. Res.-Atmos.*, 113, D19306, doi:10.1029/2008JD009943, 2008.

Rodgers, C. D.: Inverse methods for atmospheric sounding: theory and practice, Singapore,

---

**Profiles of CH<sub>4</sub>, HDO,  
H<sub>2</sub>O, and N<sub>2</sub>O**


---

J. Worden et al.

Title Page

Abstract

Introduction

Conclusions

References

Tables

Figures

◀

▶

◀

▶

Back

Close

Full Screen / Esc

Printer-friendly Version

Interactive Discussion



London, World Scientific, 2000.

Sarrat, C., Noilhan, J., Lacarrere, P., Donier, S., Lac, C., Calvet, J. C., Dolman, A. J., Gerbig, C.,  
Neisinger, B., Ciais, P., Paris, J. D., Boumard, F., Ramonet, M., and Butet, A.: Atmospheric  
CO<sub>2</sub> modeling at the regional scale: Application to the CarboEurope Regional Experiment,  
5 J. Geophys. Res.-Atmos., 112, D12105, doi:10.1029/2006JD008107, 2007.

Schneider, M., Hase, F., and Blumenstock, T.: Ground-based remote sensing of HDO/H<sub>2</sub>O ratio  
profiles: introduction and validation of an innovative retrieval approach, Atmos. Chem. Phys.,  
6, 4705–4722, doi:10.5194/acp-6-4705-2006, 2006.

Shephard, M. W., Herman, R. L., Fisher, B. M., Cady-Pereira, K. E., Clough, S. A., Payne,  
10 V. H., Whiteman, D. N., Comer, J. P., Vomel, H., Miloshevich, L. M., Forno, R., Adam, M.,  
Osterman, G. B., Eldering, A., Worden, J. R., Brown, L. R., Worden, H. M., Kulawik, S. S.,  
Rider, D. M., Goldman, A., Beer, R., Bowman, K. W., Rodgers, C. D., Luo, M., Rinsland, C. P.,  
Lampel, M., and Gunson, M. R.: Comparison of Tropospheric Emission Spectrometer nadir  
water vapor retrievals with in situ measurements, J. Geophys. Res.-Atmos., 113, D15S24,  
15 doi:10.1029/2007JD008822, 2008.

Steinwagner, J., Fueglistaler, S., Stiller, G., von Clarmann, T., Kiefer, M., Borsboom, P. P., van  
Delden, A., and Rockmann, T.: Tropical dehydration processes constrained by the season-  
ality of stratospheric deuterated water, Nature Geoscience, 3, 262–266, 2010.

Stephens, G. L. and Vane, D. G.: Cloud remote sensing from space in the era of the A-Train, J.  
20 Appl. Remote Sens., 1, 013507, doi:10.1117/1.2709703, 2007.

Stephens, B. B., Gurney, K. R., Tans, P. P., Sweeney, C., Peters, W., Bruhwiler, L., Ciais, P.,  
Ramonet, M., Bousquet, P., Nakazawa, T., Aoki, S., Machida, T., Inoue, G., Vinnichenko, N.,  
Lloyd, J., Jordan, A., Heimann, M., Shibistova, O., Langenfelds, R. L., Steele, L. P., Francey,  
R. J., and Denning, A. S.: Weak northern and strong tropical land carbon uptake from vertical  
25 profiles of atmospheric CO<sub>2</sub>, Science, 316, 1732–1735, 2007.

Su, H., Jiang, J. H., Gu, Y., Neelin, J. D., Kahn, B. H., Feldman, D., Yung, Y. L., Waters, J.  
W., Livesey, N. J., Santee, M. L., and Read, W. G.: Variations of tropical upper tropospheric  
clouds with sea surface temperature and implications for radiative effects, J. Geophys. Res.-  
Atmos., 113, D10211, doi:10.1029/2007JD009624, 2008.

30 Wofsy, S. W., S. C., Team, H. S., Team, C. M., and Team, S.: HIAPER Pole-to-Pole Obser-  
vations (HIPPO): fine-grained, global-scale measurements of climatically important atmo-  
spheric gases and aerosols, Philosophical Transactions of the Royal Society a-Mathematical  
Physical and Engineering Sciences, 369, 2073–2086, 2011.

**Profiles of CH<sub>4</sub>, HDO,  
H<sub>2</sub>O, and N<sub>2</sub>O**

J. Worden et al.

[Title Page](#)[Abstract](#)[Introduction](#)[Conclusions](#)[References](#)[Tables](#)[Figures](#)[I◀](#)[▶I](#)[◀](#)[▶](#)[Back](#)[Close](#)[Full Screen / Esc](#)[Printer-friendly Version](#)[Interactive Discussion](#)

- Worden, J., Kulawik, S. S., Shephard, M. W., Clough, S. A., Worden, H., Bowman, K., and Goldman, A.: Predicted errors of tropospheric emission spectrometer nadir retrievals from spectral window selection, *J. Geophys. Res.-Atmos.*, 109, D09308, doi:10.1029/2004JD004522, 2004.
- 5 Worden, J., Bowman, K., Noone, D., Beer, R., Clough, S., Eldering, A., Fisher, B., Goldman, A., Gunson, M., Herman, R., Kulawik, S., Lampel, M., Luo, M., Osterman, G., Rinsland, C., Rodgers, C., Sander, S., Shephard, M., and Worden, H.: Tropospheric Emission Spectrometer observations of the tropospheric HDO/H<sub>2</sub>O ratio: Estimation approach and characterization, *J. Geophys. Res.*, 111, D16309, doi:10.1029/2005JD006606, 2006.
- 10 Worden, J., Noone, D., Bowman, K., and TES science team and data contributors: Importance of rain evaporation and continental convection in the tropical water cycle, *Nature*, 445, 528–532, doi:10.1038/nature05508, 2007.

**Profiles of CH<sub>4</sub>, HDO, H<sub>2</sub>O, and N<sub>2</sub>O**

J. Worden et al.

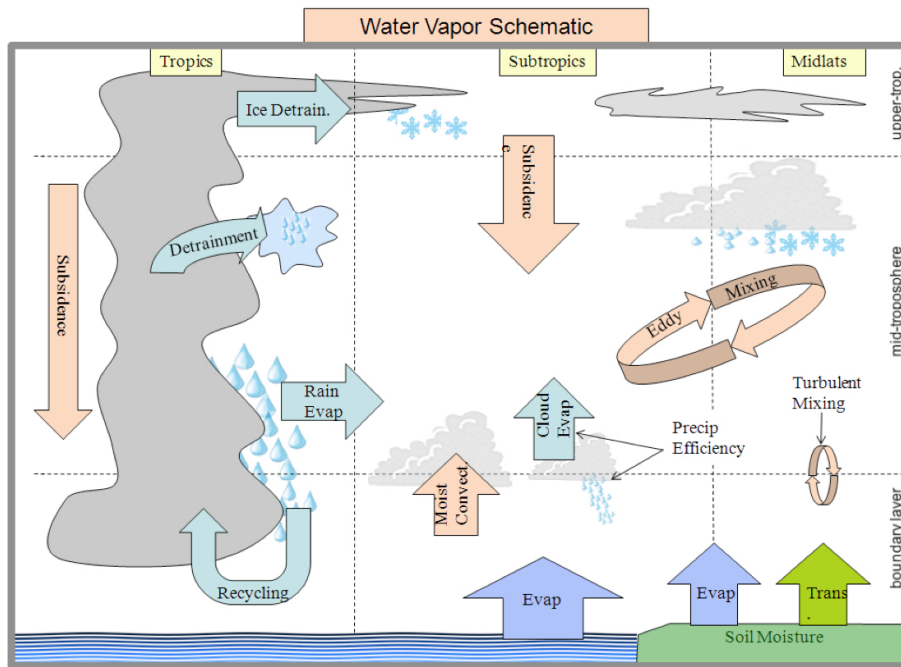


**Fig. 1a.** Sources, sinks, and processes controlling tropospheric water vapor (courtesy Derek Brown, dissertation).

Title Page

Abstract Introduction

Conclusions References

Tables Figures

◀ ▶

◀ ▶

Back Close

Full Screen / Esc

Printer-friendly Version

Interactive Discussion



## Profiles of CH<sub>4</sub>, HDO, H<sub>2</sub>O, and N<sub>2</sub>O

J. Worden et al.

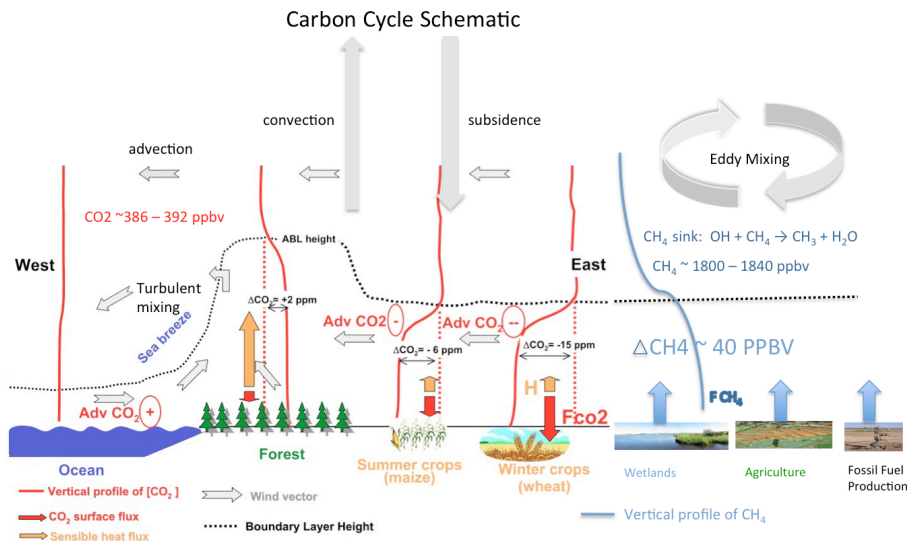
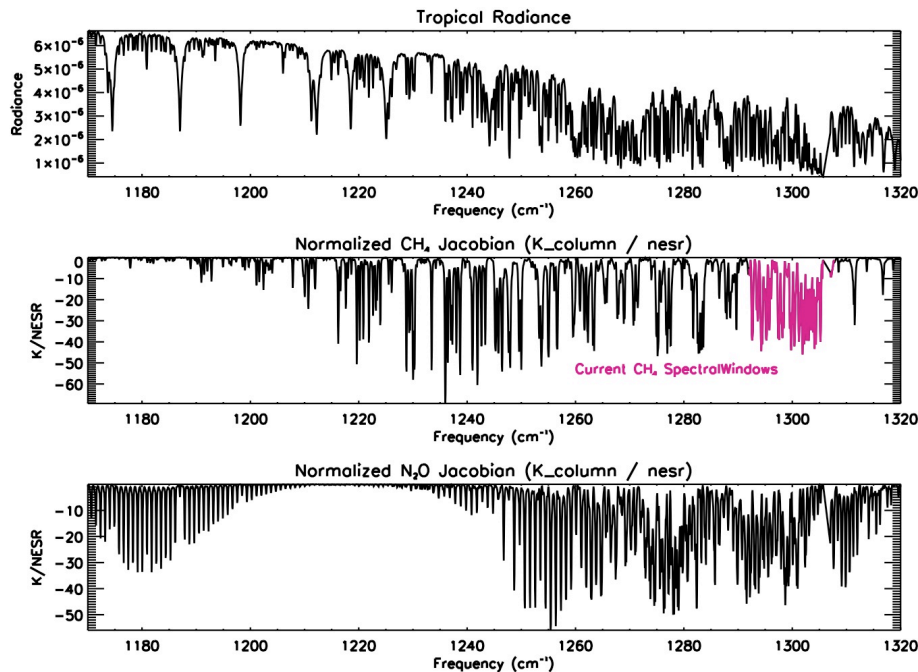


**Fig. 1b.** Sources, sinks, and processes controlling tropospheric CO<sub>2</sub> and CH<sub>4</sub> (adapted from Sarrat et al., 2007).

[Title Page](#)
[Abstract](#)
[Introduction](#)
[Conclusions](#)
[References](#)
[Tables](#)
[Figures](#)
[◀](#)
[▶](#)
[◀](#)
[▶](#)
[Back](#)
[Close](#)
[Full Screen / Esc](#)
[Printer-friendly Version](#)
[Interactive Discussion](#)


Profiles of CH<sub>4</sub>, HDO,  
H<sub>2</sub>O, and N<sub>2</sub>O

J. Worden et al.

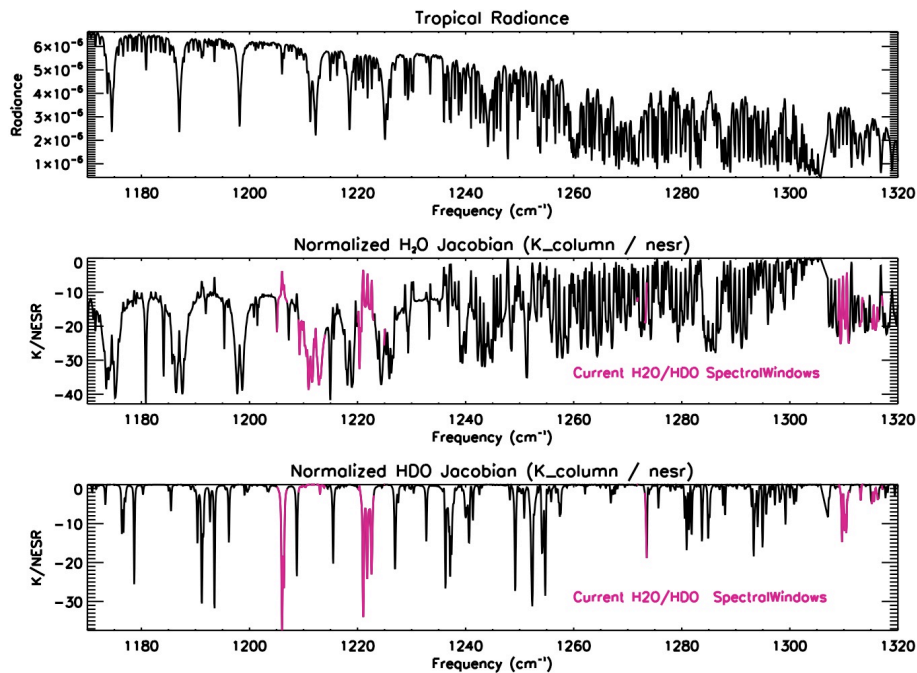


**Fig. 2a.** Top: example of radiance measured by TES over a tropical ocean scene. Middle: sensitivity of TOA radiance to (log) CH<sub>4</sub>, integrated over the whole atmospheric column and normalized by the TES NESR. Bottom: same as middle but for N<sub>2</sub>O. The red shaded area indicates the spectral region used for TES Version 6 (or less) methane retrievals.

[Title Page](#)[Abstract](#)[Introduction](#)[Conclusions](#)[References](#)[Tables](#)[Figures](#)[◀](#)[▶](#)[◀](#)[▶](#)[Back](#)[Close](#)[Full Screen / Esc](#)[Printer-friendly Version](#)[Interactive Discussion](#)

**Profiles of CH<sub>4</sub>, HDO,  
H<sub>2</sub>O, and N<sub>2</sub>O**

J. Worden et al.

**Fig. 2b.** Same as in Fig. 2a but for H<sub>2</sub>O and HDO.

Title Page

Abstract

Introduction

Conclusions

References

Tables

Figures

◀

▶

◀

▶

Back

Close

Full Screen / Esc

Printer-friendly Version

Interactive Discussion



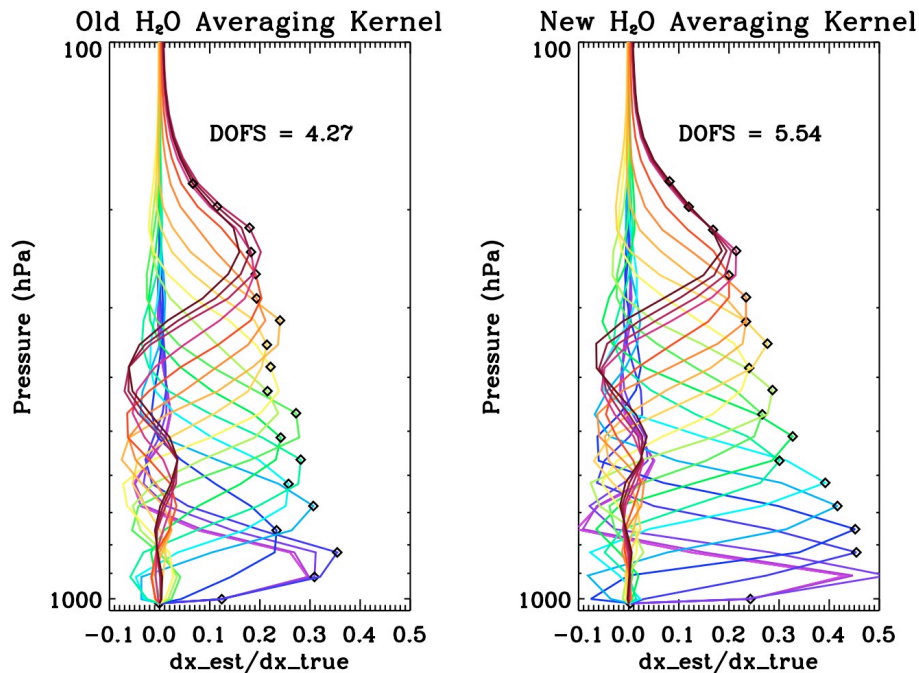


**Fig. 3a.** Averaging kernels for a TES water retrieval using old (spectral windows shown in Fig. 2b) and new (using almost all the radiance shown in Fig. 2b). The diamonds indicate the pressure level for the averaging kernel. Color coding is to help the reader follow the variability of each averaging kernel with pressure.

[Title Page](#)[Abstract](#)[Introduction](#)[Conclusions](#)[References](#)[Tables](#)[Figures](#)[◀](#)[▶](#)[◀](#)[▶](#)[Back](#)[Close](#)[Full Screen / Esc](#)[Printer-friendly Version](#)[Interactive Discussion](#)

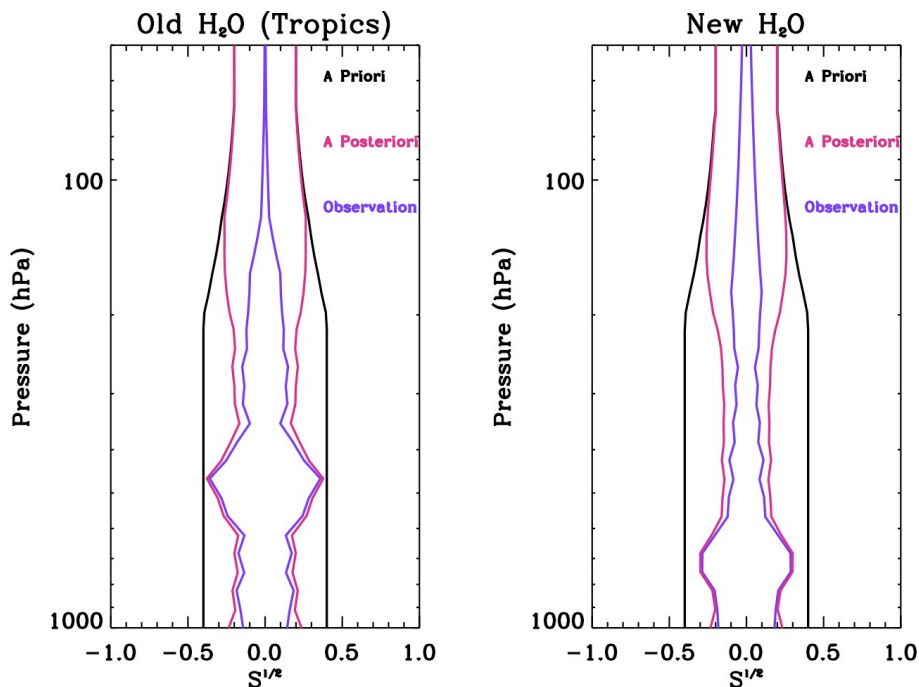


**Fig. 3b.** The square root of the diagonal of the error covariances. Observation error includes uncertainties from jointly retrieved parameters affecting the radiance and error due to noise. The a posteriori error is the sum of the observation error and smoothing error.

[Title Page](#)[Abstract](#)[Introduction](#)[Conclusions](#)[References](#)[Tables](#)[Figures](#)[◀](#)[▶](#)[◀](#)[▶](#)[Back](#)[Close](#)[Full Screen / Esc](#)[Printer-friendly Version](#)[Interactive Discussion](#)

Profiles of CH<sub>4</sub>, HDO,  
H<sub>2</sub>O, and N<sub>2</sub>O

J. Worden et al.

Title Page

Abstract

Introduction

Conclusions

References

Tables

Figures

◀

▶

◀

▶

Back

Close

Full Screen / Esc

Printer-friendly Version

Interactive Discussion

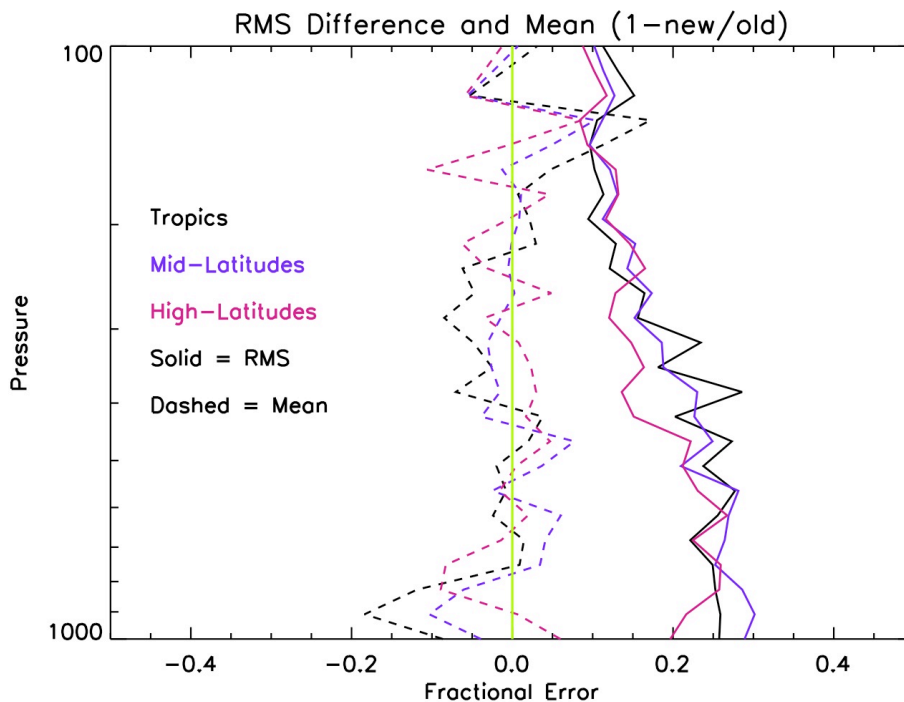


**Fig. 4.** The RMS and Mean of the fractional difference between the new and old TES H<sub>2</sub>O retrievals. Tropics indicate all latitudes less than 20 degrees (North and South). Mid-latitudes are between 20 and 50 degrees (North and South) and High Latitudes are all latitudes greater than 50 degrees North (to avoid Antarctica where retrievals have very low sensitivity).

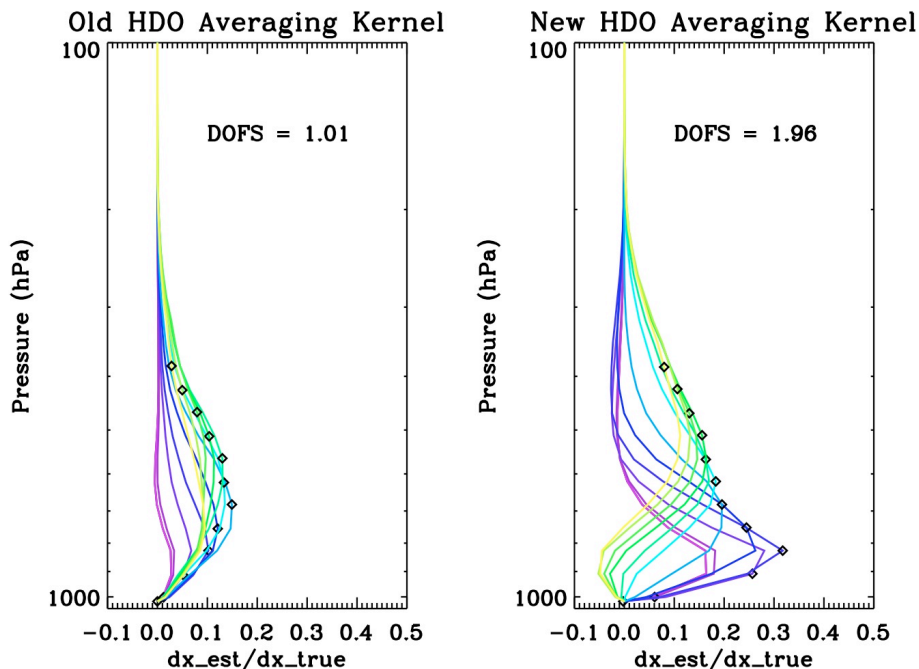


**Fig. 5a.** Averaging kernel for the old and new HDO TES retrievals. As in Fig. 3a, the symbols and colors indicate the pressure level and variation with pressure of each row of the averaging kernel matrix.

[Title Page](#)[Abstract](#)[Introduction](#)[Conclusions](#)[References](#)[Tables](#)[Figures](#)[◀](#)[▶](#)[◀](#)[▶](#)[Back](#)[Close](#)[Full Screen / Esc](#)[Printer-friendly Version](#)[Interactive Discussion](#)

## Profiles of CH<sub>4</sub>, HDO, H<sub>2</sub>O, and N<sub>2</sub>O

J. Worden et al.

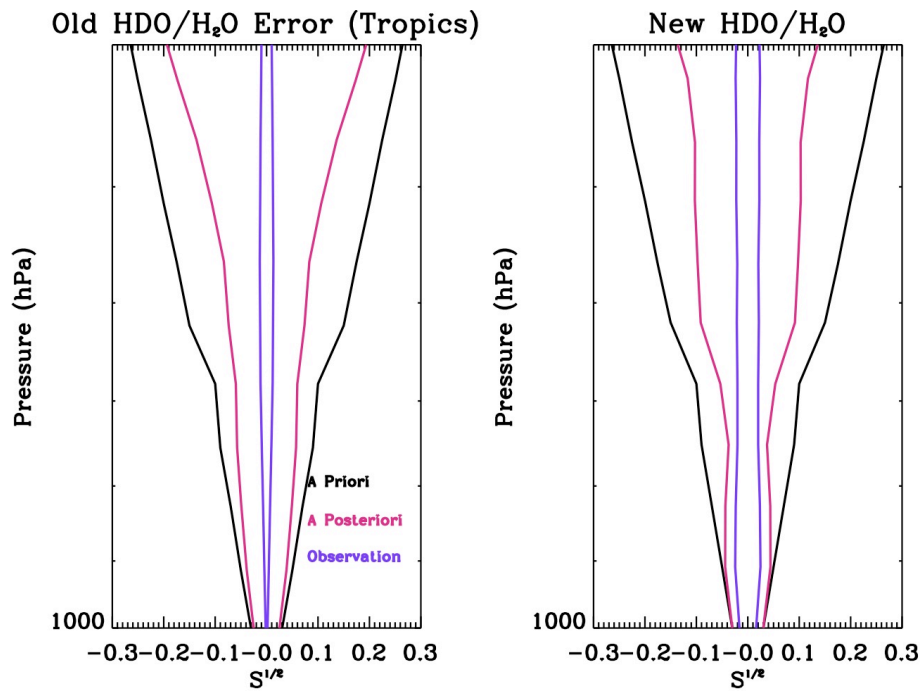


**Fig. 5b.** Same as in Fig. 3b but for the HDO/H<sub>2</sub>O ratio.

Title Page	
Abstract	Introduction
Conclusions	References
Tables	Figures
◀	▶
◀	▶
Back	Close
Full Screen / Esc	
Printer-friendly Version	
Interactive Discussion	



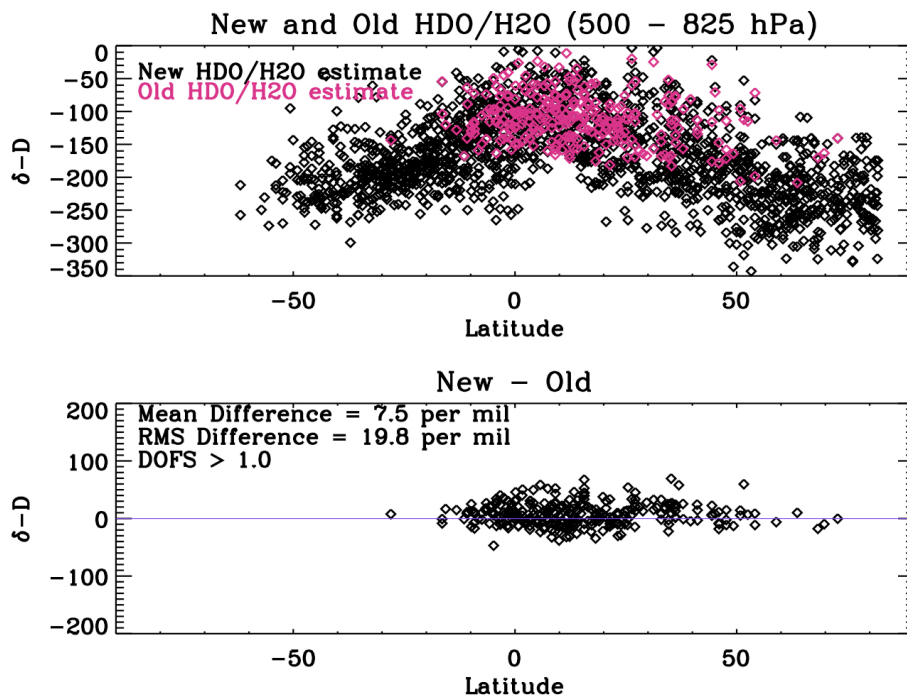


**Fig. 6.** Top: comparison of the new and old (Version 6) HDO/H<sub>2</sub>O estimates. A DOFS threshold of 0.7 is used for the data in the top panel for both releases. Bottom: difference between old and new HDO/H<sub>2</sub>O estimates for the overlapping data shown in the top panel.  $\delta - D = 1000(\text{HDO}/\text{H}_2\text{O}/3.11 \times 10^{-4} - 1)$ .

[Title Page](#)[Abstract](#)[Introduction](#)[Conclusions](#)[References](#)[Tables](#)[Figures](#)[◀](#)[▶](#)[◀](#)[▶](#)[Back](#)[Close](#)[Full Screen / Esc](#)[Printer-friendly Version](#)[Interactive Discussion](#)

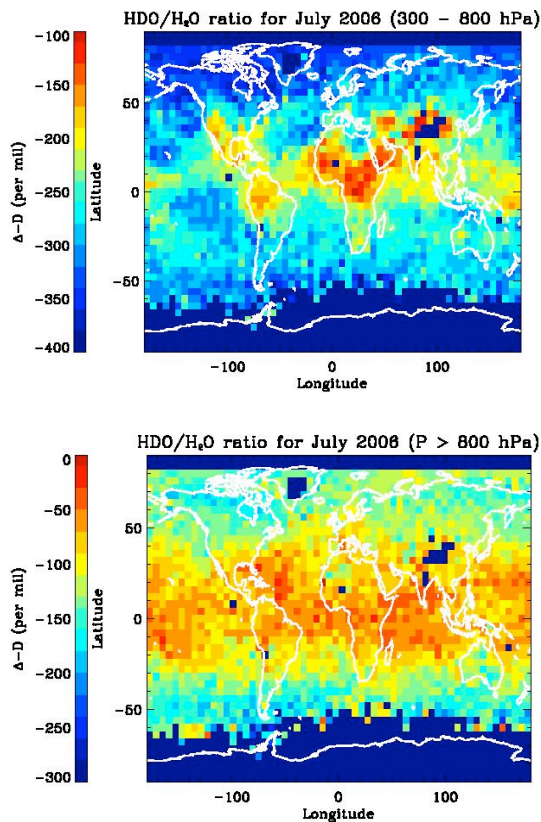


**Fig. 7.** Bottom panel: averaged TES HDO/H<sub>2</sub>O estimates for pressures greater than 800 hPa. Top panel: averaged TES HDO/H<sub>2</sub>O estimates for pressures between 300 and 800 hPa.

Title Page

Abstract

Introduction

Conclusions

References

Tables

Figures

◀

▶

◀

▶

Back

Close

Full Screen / Esc

Printer-friendly Version

Interactive Discussion



Profiles of CH<sub>4</sub>, HDO,  
H<sub>2</sub>O, and N<sub>2</sub>O

J. Worden et al.

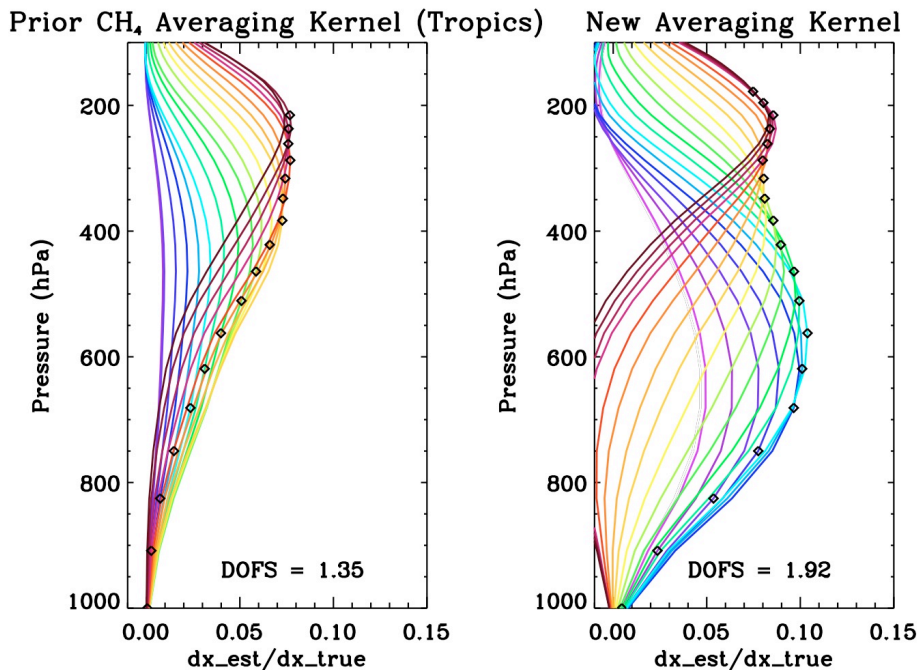


**Fig. 8.** Averaging kernels for the old (Version 6 or less) TES methane retrievals and the new TES methane retrievals. The diamonds indicate the pressure level for the averaging kernel. Color coding is to help the reader follow the variability of each averaging kernel with pressure.

[Title Page](#)[Abstract](#)[Introduction](#)[Conclusions](#)[References](#)[Tables](#)[Figures](#)[◀](#)[▶](#)[◀](#)[▶](#)[Back](#)[Close](#)[Full Screen / Esc](#)[Printer-friendly Version](#)[Interactive Discussion](#)

Profiles of CH<sub>4</sub>, HDO,  
H<sub>2</sub>O, and N<sub>2</sub>O

J. Worden et al.

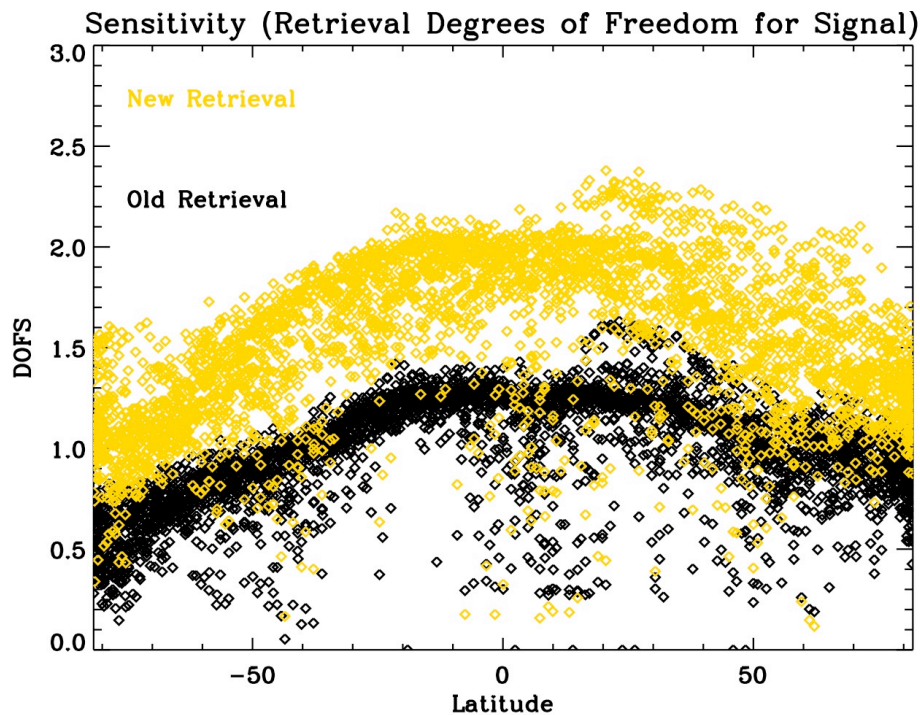
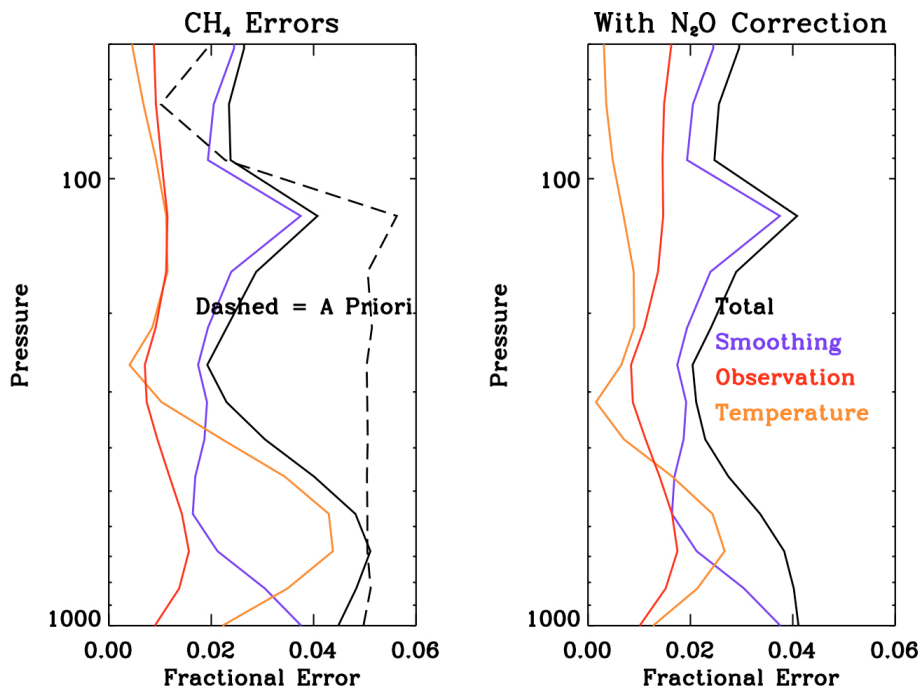


Fig. 9. DOFS for the new methane retrieval (yellow) and the old methane retrieval (black).

[Title Page](#)[Abstract](#)[Introduction](#)[Conclusions](#)[References](#)[Tables](#)[Figures](#)[◀](#)[▶](#)[◀](#)[▶](#)[Back](#)[Close](#)[Full Screen / Esc](#)[Printer-friendly Version](#)[Interactive Discussion](#)



**Fig. 10.** Error budget for the methane estimate before and after correcting the methane profile with the ratio of the TES estimated N<sub>2</sub>O and the TES N<sub>2</sub>O a priori. Observation error is the sum of the measurement error related to noise and due to jointly estimated parameters. The total error is the sum of the smoothing, observation, and temperature error.

[Title Page](#)[Abstract](#)[Introduction](#)[Conclusions](#)[References](#)[Tables](#)[Figures](#)[◀](#)[▶](#)[◀](#)[▶](#)[Back](#)[Close](#)[Full Screen / Esc](#)[Printer-friendly Version](#)[Interactive Discussion](#)

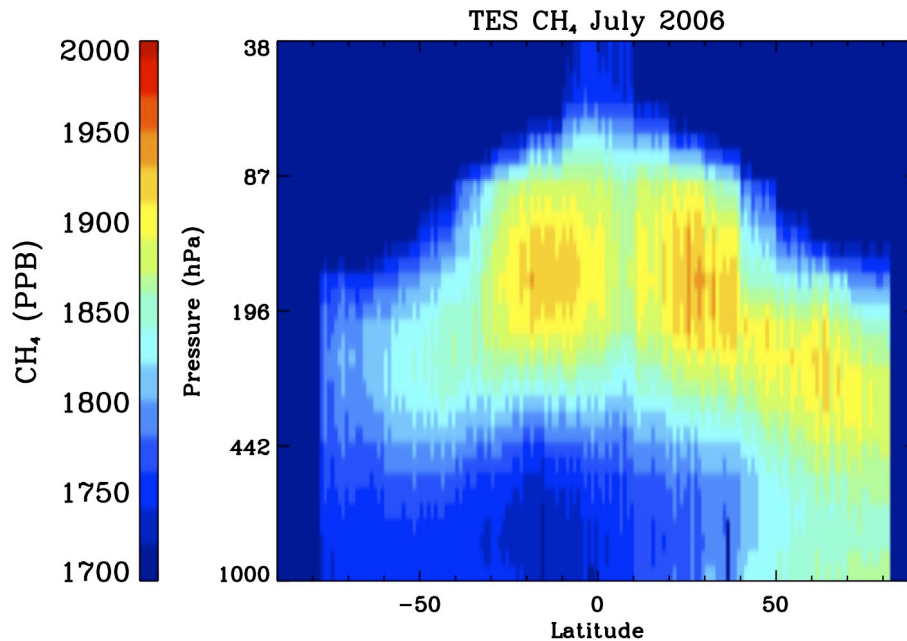


Fig. 11. TES tropospheric methane, averaged over all longitudes.

**Profiles of CH<sub>4</sub>, HDO, H<sub>2</sub>O, and N<sub>2</sub>O**

J. Worden et al.

Title Page

Abstract Introduction

Conclusions References

Tables Figures

◀ ▶

◀ ▶

Back Close

Full Screen / Esc

Printer-friendly Version

Interactive Discussion



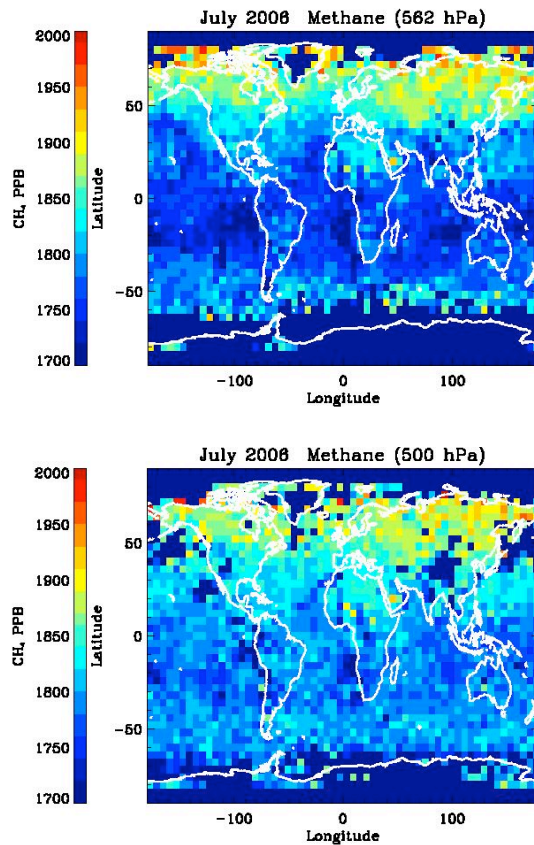


**Fig. 12.** Top: TES estimated methane at 562 hPa. Bottom: TES estimated methane at approximately 500 hPa using an “information” averaging approach.

Title Page

Abstract

Introduction

Conclusions

References

Tables

Figures

◀

▶

◀

▶

Back

Close

Full Screen / Esc

Printer-friendly Version

Interactive Discussion



## Profiles of CH<sub>4</sub>, HDO, H<sub>2</sub>O, and N<sub>2</sub>O

J. Worden et al.

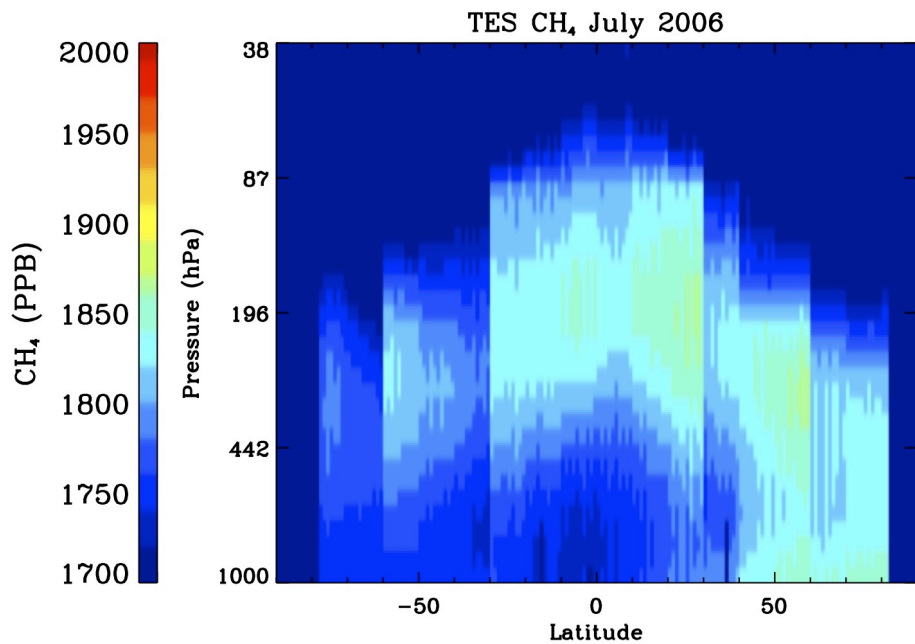


**Fig. 13.** TES CH<sub>4</sub> as a function of latitude after applying N<sub>2</sub>O correction.

Title Page	
Abstract	Introduction
Conclusions	References
Tables	Figures
◀	▶
◀	▶
Back	Close
Full Screen / Esc	
Printer-friendly Version	
Interactive Discussion	



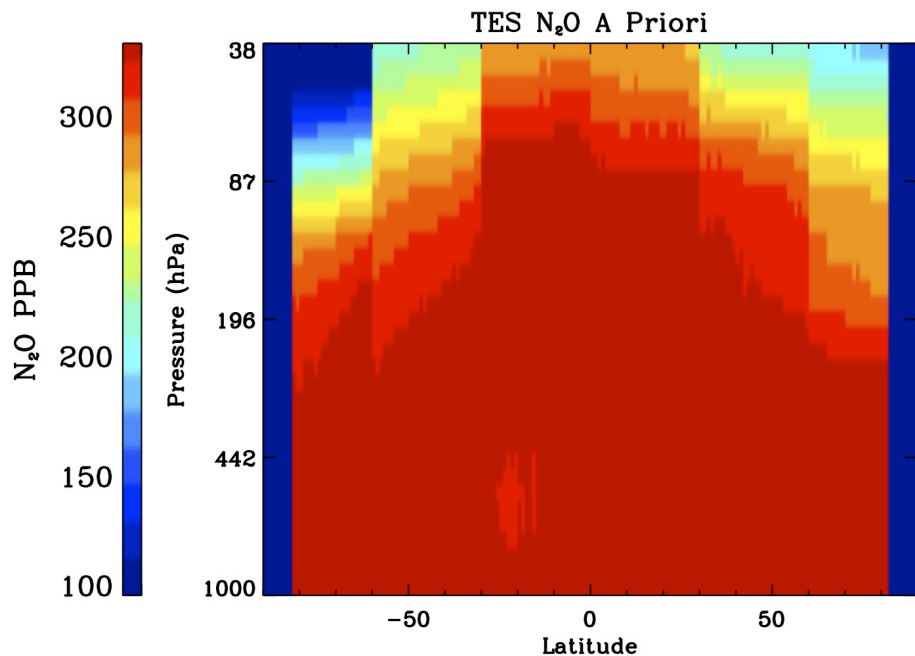


Fig. 14. N<sub>2</sub>O a priori distribution used for the TES N<sub>2</sub>O estimates.

Discussion Paper | Discussion Paper | Discussion Paper | Discussion Paper | Discussion Paper

# AMTD

4, 6679–6721, 2011

## Profiles of CH<sub>4</sub>, HDO, H<sub>2</sub>O, and N<sub>2</sub>O

J. Worden et al.

<a href="#">Title Page</a>	
<a href="#">Abstract</a>	<a href="#">Introduction</a>
<a href="#">Conclusions</a>	<a href="#">References</a>
<a href="#">Tables</a>	<a href="#">Figures</a>
<a href="#">◀</a>	<a href="#">▶</a>
<a href="#">◀</a>	<a href="#">▶</a>
<a href="#">Back</a>	<a href="#">Close</a>
<a href="#">Full Screen / Esc</a>	
<a href="#">Printer-friendly Version</a>	
<a href="#">Interactive Discussion</a>	

